Fermions and bosons : excitons in strongly correlated materials

Rademaker, L.

5
Exciton condensation in the $t-J$ model

The bosonic exciton $t-J$ model derived in the previous section allows for exciton condensation. In this phase, a remarkable cooperation effect arises between the exciton and spin dynamics. In section 5.1 we discuss this specific feature of the strongly correlated exciton condensate. We conclude our study of the exciton $t-J$ model by constructing the full phase diagram in section 5.2.

Completely opposite to the frustration effect presented in section 4.2 is the cooperation between excitons and spins that arises in the context of a **finite densities of excitons**.[1] Much effort has been devoted to create equilibrium finite exciton densities using conventional semiconductors,[2] while exciton condensation has been demonstrated in coupled semiconductor 2DEGs.[3] In strongly correlated p/n heterostructures,[4] however, formation of finite exciton densities is still far from achieved, although recent developments on oxide interfaces indicate exciting potential (see for example Pentcheva et al., 2010). Besides the closely coupled p- and n-doped conducting interface-layers in these $SrTiO_3$-$LaAlO_3$-$SrTiO_3$ heterostructures, further candidates would be closely coupled p- and n-doped cuprates, such as $YBa_2Cu_3O_{7-x}$ or $La_{2-x}Sr_xCuO_4$ with $Nd_{2-x}Ce_xCuO_4$. The feasibility of this has already been experimentally demonstrated, e.g. in Takeuchi et al., 1995, but the exact interface effects need to be investigated in more detail, both experimentally as well as theoretically.

The nontrivial cooperation effect between excitons and spins is only visible in the **exciton condensate phase doped into a Mott**

[1] Ribeiro et al., 2006; and Millis and Schlom, 2010

[2] Moskalenko and Snoke, 2000

[3] Eisenstein and MacDonald, 2004; Butov, 2007; and High et al., 2012

[4] One can wonder whether such physics is already at work in the four-layer material $Ba_2Ca_3Cu_4O_8F_2$ where self-doping effects occur creating simultaneously p and n-doped layers, Chen et al., 2006.

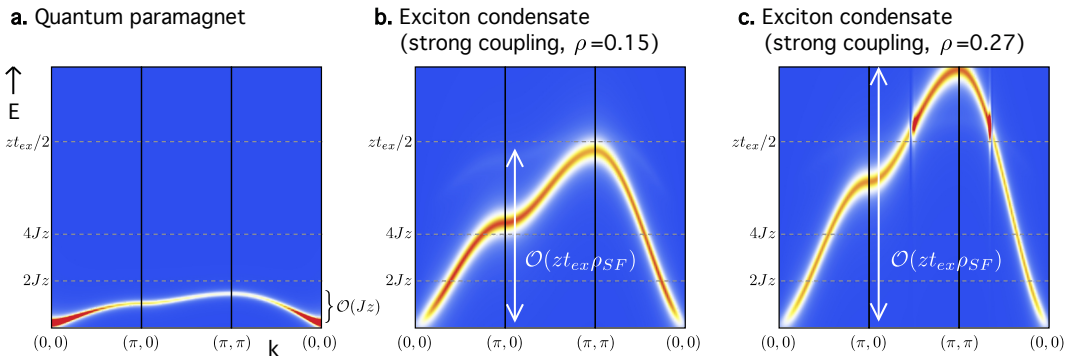

Figure 5.1: The absorptive part of the dynamical magnetic susceptibility $\chi''(\mathbf{q},\omega)$ in a Mott insulating bilayer (a) doped to become an exciton condensate (b,c). **a:** The spectrum of a Mott insulating bilayer with the same gap as the exciton condensates of figure b and c. The bandwidth of the triplon mode is of the order Jz. **b.** In the presence of the exciton condensate, the magnetic excitation spectrum consists of propagating triplets. Instead of the small $\mathcal{O}(Jz)$ bandwidth, the triplet has now an enhanced bandwidth $\mathcal{O}(zt_{ex}\rho_{SF})$, proportional to the superfluid density. This result is computed using a linear spin wave approximation, using model parameters $t_{ex} = 2, J = 0.125, \alpha = 0.04$ and $\rho = 0.15$. **c.** The same result as in b, but now with a higher exciton density $\rho = 0.27$. The triplet mode bandwidth is seen to scale with the exciton superfluid density.

[5] Ament et al., 2011

[6] Dean et al., 2012

This section 5.1 is based on Rademaker et al., 2013a.

insulating bilayer. The non-condensed electrons form a quantum paramagnet, which has as elementary magnetic excitations the triplet modes (triplons, see the book by Sachdev, 2011). One expects that the bandwidth of the triplons is proportional to the superexchange energy J. However, interlayer exciton condensation now leads to a drastic **increase of the triplon bandwidth**. In this section we show that this enhancement is rooted in the triplons 'borrowing' itineracy from the exciton condensate. The resulting bandwidth turns out to be proportional to the superfluid density, as is shown in figure 5.1. In principle, this enhancement can be detected by measurements of the dynamical magnetic susceptibility. It appears unlikely that such bilayer exciton systems can be manufactured in bulk form which is required for neutron scattering, while there is a real potential to grow these using thin layer techniques. Therefore the detection of the triplon bandwidth enhancement forms a realistic challenge for resonant inelastic X-ray scattering (RIXS)[5] measurements with its claimed sensitivity for interface physics.[6]

5.1 *Enhanced spin itineracy in the exciton condensate*

Let us now introduce the **strongly correlated exciton condensate** is somewhat more detail. As mentioned above, the exciton condensate is the result of the direct interlayer Coulomb attraction, in stark contrast to the retarded phonon mediated electron-electron pairing in superconductors. Consequently, the pairing mechanism

is remarkably simple and in the absence of spin-orbit coupling or magnetization the excitons are a singlet pair. The resulting **condensate wavefunction** has the standard BCS-form,

$$|\Psi\rangle = \prod_{\mathbf{k}\sigma} \left(u_{\mathbf{k}} + v_{\mathbf{k}} c^{\dagger}_{\mathbf{k}1\sigma} c_{\mathbf{k}2\sigma} \right) |\Psi_0\rangle \tag{5.1}$$

where $|\Psi_0\rangle$ is the ground state without excitons, $c^{\dagger}_{\mathbf{k}1\sigma}$ creates an electron in the first layer and $c_{\mathbf{k}2\sigma}$ creates a hole in the second layer with opposite spin. The order parameter is independent of spin

$$\Delta_{\mathbf{k}} = u_{\mathbf{k}} v_{\mathbf{k}} = \langle c^{\dagger}_{\mathbf{k}1\sigma} c_{\mathbf{k}2\sigma} \rangle. \tag{5.2}$$

Recall from section 2.1 that the anomalous interlayer tunneling serves as a direct probe of the order parameter.[7]

[7] Eisenstein and MacDonald, 2004

The enhancement of the triplet mode is an effect that only occurs in the regime of strong electron-electron interactions. The realization of exciton condensates has been suggested to be possible in strongly correlated materials[8] where the cuprates[9] would serve as ideal candidate systems. In Mott insulators electrons localize due to interactions and only their spin remains as a degree of freedom. Such bilayers (figure 4.1) are described by the **bilayer Heisenberg model**[10] introduced in section 4.1, defined by

[8] Ribeiro et al., 2006; and Millis and Schlom, 2010

[9] Imada et al., 1998; and Lee et al., 2006

[10] Manousakis, 1991; and Chubukov and Morr, 1995

$$H_J = J \sum_{\langle ij \rangle, \ell} \mathbf{s}_{i\ell} \cdot \mathbf{s}_{j\ell} + J_{\perp} \sum_{i} \mathbf{s}_{i1} \cdot \mathbf{s}_{i2}. \tag{5.3}$$

The operators $\mathbf{s}_{i\ell}$ denote the spin of a particle on site i in layer ℓ, and via this mechanism of superexchange spin excitations can propagate. The superexchange parameters J are related to the bare electron hopping t by the strong coupling perturbation theory of section 4.1, recall $J = 4t^2/U$ and $J_{\perp} = 4t_{\perp}^2/U$ with U the onsite repulsion. This model represents a paramagnet when $J_{\perp} \gg J$, thus favoring singlet configurations on each interlayer rung. The excitation spectrum consists of propagating triplet modes, with a dispersion $\omega_{\mathbf{k}} = Jz\sqrt{\alpha(\alpha - \gamma_{\mathbf{k}})}$ where $\alpha = J_{\perp}/Jz$ and z is the lattice coordination number. Hence the bandwidth of these triplets in the absence of exciton condensation is set by the superexchange parameter J. We compute the interlayer dynamical magnetic susceptibility[11]

[11] Bruus and Flensberg, 2004

$$\chi_{ij}(\tau) = \langle T_{\tau}(s^{-}_{i1}(\tau) - s^{-}_{i2}(\tau))(s^{+}_{j1} - s^{+}_{j2}) \rangle \tag{5.4}$$

using the well-tested **linear spin wave theory**.[12] The imaginary

[12] This is further elaborated upon in section 5.2.4. See also Manousakis, 1991 and Chubukov and Morr, 1995.

part χ'', which describes the absorption, is in principle measurable by RIXS[13] and a typical spectrum is shown in figure 5.1a.

[13] Ament et al., 2011

As for the case of normal carriers in a doped Mott insulator, the nature of the exciton system is drastically different from what is found in uncorrelated semiconductors. The Mott insulator cannot be described by band theory, and instead electron- and hole-doping corresponds with the creation of double occupied sites (doublons) and empty sites (holons), respectively. The doublons and holons attract each other via the Coulomb attraction and can thus form doublon-holon pairs: the strong coupling limit of the exciton. Since in the Mott bilayer all interactions are strong, the relevant case is to assume strong exciton binding such that excitons can be treated as local pairs and the condensation occurs in the BEC sense rather than in the weak coupling BCS sense.[14]

[14] The BCS theory of electron-hole pairing is discussed in section 3.2.

To describe such a doublon-holon pair in a Mott bilayer, we can express the exciton hopping in terms of interlayer rung states: the exciton $|E\rangle$ and the four possible interlayer spin states $|s\ m\rangle$. Recall that the motion of an exciton is governed by[15]

[15] See section 4.1.

$$H_K = -t_{ex} \sum_{\langle ij \rangle} |E\rangle_j \left(\sum_{sm} |s\ m\rangle_i \langle s\ m|_j \right) \langle E|_i. \tag{5.5}$$

The exciton hopping energy t_{ex} can be related to the electron hopping via perturbation theory, which gives $t_{ex} = t^2/V$ where V equals the binding energy of an exciton.

The system describing coexistence of spins and excitons, given by equations (5.3) and (5.5), is equivalent to a hard-core boson system, reminiscent of attempts to describe cuprate superconductivity using only bosons such as the $SO(5)$ theory of the $t-J$ model.[16] In contrast to these theories, for the excitons in Mott bilayers the mapping onto bosonic physics is fully controlled. The ground state of the 'exciton $t-J$ model' can straightforwardly be found using a $SU(5)$ coherent state. In the next section 5.2 we study this in detail, finding that the dynamical frustration between excitons and spins causes large parts of the phase diagram to be dominated by phase separation. As long as the exciton hopping t is bigger than the exciton-exciton repulsion we find an exciton superfluid as the ground state, where the spins form interlayer singlets. In principle there can be sign problems but these drop out rigorously for this singlet ground state.

[16] Zhang, 1997

The **strongly correlated exciton condensate wavefunction** is

now

$$|\Psi\rangle = \prod_i \left(\sqrt{\rho}\,|E\rangle_i + \sqrt{1-\rho}\,|0\;0\rangle_i\right) \tag{5.6}$$

where $|0\;0\rangle$ is the interlayer singlet spin configuration. Indeed, when we set $\Delta_{\mathbf{k}}$ to be independent of momentum the earlier wavefunction (5.1) reduces to the above equation.

Since we are dealing with hard-core bosons forming a mean field ground state, the magnetic excitation spectrum can be computed with linear spin wave theory. We employ the Heisenberg equations of motion[17] which are decoupled exploiting the ground state expectation values.[18] The resulting dynamical magnetic susceptibilities $\chi''(\mathbf{q},\omega)$ are shown in figure 5.1, for two choices of exciton density $\rho = 0.15$ and $\rho = 0.27$.

[17] See section 5.2.4.

[18] Zubarev, 1960; and Oles et al., 2000

These figures illustrate the central result of this section: compared to the undoped system (figure 5.1a) we find that the **triplon bandwidth is greatly enhanced** (figures 5.1b and c). The mechanism is actually similar to that in slave-boson theories,[19] where four-operator products $b^\dagger b f^\dagger f$ are decoupled as $\langle b^\dagger\rangle\langle b\rangle f^\dagger f$ yielding kinetic energy for the f-excitations. For Mott bilayers, we can explicitly introduce Fock operators for the exciton $e^\dagger = |E\rangle\langle 0|$ and the triplet $t^\dagger = |1m\rangle\langle 0|$. This implies that the exciton-spin interaction term (4.26) can be written as

[19] Lee et al., 2006

$$-t_{ex}\sum_{\langle ij\rangle} e_j^\dagger e_i t_i^\dagger t_j. \tag{5.7}$$

This is a higher order exchange term, which at first sight seems to be irrelevant for the bandwidth of the triplet. However, when the exciton condensate sets in, the operator $e^\dagger$ obtains an expectation value $\langle e^\dagger\rangle = \sqrt{\rho_{\mathrm{SF}}}$, where ρ_{SF} is the condensate density. Consequently this exchange term turns into an effective triplet hopping term

$$-t_{ex}\rho_{\mathrm{SF}}\sum_{\langle ij\rangle} t_i^\dagger t_j. \tag{5.8}$$

The explains why the bandwidth of the triplet excitations is increased by an amount of order $z t_{ex}\rho_{\mathrm{SF}}$.

Surely, we made the argument that this effect leads to a dramatic increase of the bandwidth, for which we have implicitly assumed that t_{ex} is larger than J. Now the exciton hopping energy is related to the electron hopping by $t_{ex} = t^2/V$, while the spin superexchange satisfies $J = 2t^2/U$ where U is the onsite Coulomb

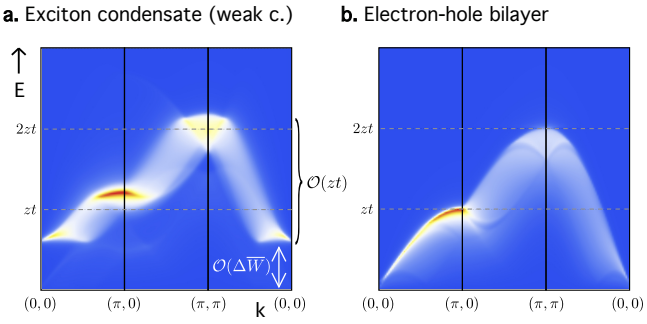

Figure 5.2: The absorptive part of the dynamical magnetic susceptibility $\chi''(\mathbf{q},\omega)$ in the weak-coupling limit of both the exciton binding energy and electron-electron interactions. **a:** The magnetic susceptibility is also in the exciton condensate phase dominated by the Lindhard continuum. This is qualitatively different from the triplons found in the strong coupling limit of figure 5.1. Model parameters are $\xi_{1\mathbf{k}} = -zt\gamma_{\mathbf{k}} - \mu = -\xi_{2\mathbf{k}}$, $t_\perp = 0.05zt$, $\mu = -0.8zt$ and $\Delta\overline{W} = t$. **b:** For comparison we computed the $\chi''(\mathbf{q},\omega)$ in an electron-hole bilayer without exciton condensation.

repulsion. Since for obvious reasons $U > V$, we find that indeed the dominant scale controlling the triplon bandwidth is $zt_{ex}\rho_{\rm SF}$ yielding the predicted bandwidth enhancement.

Since the exciton condensate ground state is independent of the interaction strength, one can **in principle adiabatically continue** the strong coupling results to the weak coupling limit. However, in this limit the magnetic susceptibility as shown in figure 5.2 has a fundamentally different origin. Only with strong interactions the electrons are localized and a true spin degree of freedom arises. This is not the case for weak coupling, where the spin response is still dominated by the Lindhard continuum. The propagation scale of the triplet excitations is now set just by the dispersion of the noninteracting electrons.

To illustrate this point we compute the dynamic magnetic susceptibility for the **weak coupling case** where we depart from a band structure of electrons and holes

$$H_K = \sum_{\mathbf{k}\sigma} \left(\xi_{1\mathbf{k}} c^\dagger_{1\mathbf{k}\sigma} c_{1\mathbf{k}\sigma} + \xi_{2\mathbf{k}} c^\dagger_{2\mathbf{k}\sigma} c_{2\mathbf{k}\sigma} \right) \tag{5.9}$$

plus a weak interlayer tunneling

$$H_\perp = -t_\perp \sum_{\mathbf{k}\sigma} \left(c^\dagger_{1\mathbf{k}\sigma} c_{2\mathbf{k}\sigma} + c^\dagger_{2\mathbf{k}\sigma} c_{1\mathbf{k}\sigma} \right) \tag{5.10}$$

where $\xi_{\ell\mathbf{k}}$ is the band structure of the holes or electrons, depending on the layer. For simplicity, we take $\xi_{1\mathbf{k}} = -zt\gamma_{\mathbf{k}} - \mu = -\xi_{2\mathbf{k}}$ on a square lattice, so that in both layers there is an equal sized Fermi surface with opposite Fermi velocities. The interlayer hopping $t_\perp \ll t$ is assumed to be small given the insulator in between the layers. Both in-plane and the interlayer interactions are given by

the Coulomb interaction

$$H_V = \sum_{ij\ell\sigma\sigma'} V_{ij} n_{i\ell\sigma} n_{j\ell\sigma'} + \sum_{ij\sigma\sigma'} W_{ij} n_{i1\sigma} n_{j2\sigma'}, \qquad (5.11)$$

where $V_{ij} \propto |r_i - r_j|^{-1}$ and the interlayer Coulomb includes the interlayer distance d, hence $W_{ij} \propto \left((r_i - r_j)^2 + d^2\right)^{-1/2}$. The effects of these interactions are taken into account using the random phase approximation (RPA).[20] In the bilayer case, one needs to extend the usual RPA expression $\chi = \chi_0/(1 - V_q\chi_0)$ to include both intra- and interlayer interactions and bare susceptibilities χ_0.

[20] Bruus and Flensberg, 2004

At some critical temperature the electron-hole bilayer has an instability towards exciton condensation. Based on the standard BCS theory[21] we single out the interactions responsible for the singlet exciton pairing and perform a standard mean field decoupling using our earlier order parameter ansatz (5.2). Let us fix the order parameter at a value of, say, $\Delta\overline{W} = t$. Using the aforementioned RPA expansion we compute the resulting magnetic excitation spectrum shown in figure 5.2a. This spectrum is reminiscent of our strong coupling results of figure 5.1. But instead of the renormalization of the triplet bandwidth, the magnetic excitations closely follow the Bogolyubov quasiparticle spectrum. In fact, the dynamic magnetic susceptibility in the weak coupling limit can be best understood as a gapped variation of the result in absence of a condensate, shown in figure 5.2b. In weak coupling, the gross features of the magnetic excitation spectrum therefore look similar with or without the exciton condensate, whereas the dramatic increase of the overall energy scale of the magnetic excitations is only present in the strong correlations limit.

[21] This is done extensively in section 3.2. See also Bardeen et al., 1957 and De Gennes, 1999.

In conclusion, we have shown explicitly that in a Mott bilayer the **bandwidth of the magnetic excitations is strongly enhanced by the presence of an exciton condensate**. We emphasize that this dynamic enhancement is quite unusual: the interplay between magnetic and charge degrees of freedom most commonly leads to frustration effects such as found in the previous section 4.2. Paradoxically, this effect turns around dealing with excitons in Mott insulators under the condition that they condense. This can promote the propagation of spin.

5.2 *Finite exciton densities: the full phase diagram*

This section is based on Rademaker et al., 2013b.

To conclude our analysis of the bilayer exciton $t-J$ model we will now derive its full **ground state phase diagram**. This can be done since both excitons and spins act as bosons, which is much more tractable than the fermionic doped Mott insulator physics. However, not all 'fermion-like' signs are eliminated: there are still left-over signs of the phase-string type.[22] In section 4.1.4 we show that collinear spin order is a sufficient condition for these signs to cancel out, leaving a truly bosonic dynamics controlling the ground state and long wavelength physics. This is very similar to the 'spin-orbital' physics described by Kugel-Khomskii type models,[23] which can be viewed after all as describing d-d excitons interacting with spins. Also the lattice implementations[24] of the SO(5) model[25] for (cuprate) superconductivity are in this family of bosonic theories.

[22] Weng, 2007

[23] Kugel and Khomskii, 1982

[24] van Duin and Zaanen, 2000

[25] Zhang, 1997

Such bosonic problems can be handled with standard (semi-classical) **mean field theory**. In most bilayer exciton set-ups, such as the quantum Hall bilayers or the pumped systems, there is no controllable equilibrium exciton density. In these cases one can hardly speak of the exciton density as a conserved quantity, and exciton condensation in the sense of spontaneously broken $U(1)$ symmetry is impossible.[26] However, in Mott insulators the dopant density per layer could be fixed by, for example, chemical doping. The effective exciton chemical potential is then by definition large compared to the recombination rate. Effectively, the excitons are at finite density in equilibrium and hence **true spontaneous** $U(1)$ **symmetry breaking is possible** in the Mott insulating bilayer at zero temperature.

[26] Snoke, 2006

Besides the exciton superfluid phase one anticipates a **plethora of competing orders**, as is customary in strongly correlated materials. At zero exciton density the bilayer Heisenberg system exhibits already interesting magnetic behavior. Departing from the antiferromagnet for small rung coupling it turns via an $O(3)$-QNLS quantum phase transition into an 'incompressible quantum spin liquid' for larger rung couplings that can be viewed as a continuation of pair singlets ('valence bonds') stacked on the rungs.[27] The natural competitor of the exciton superfluid at finite density is the exciton crystal and one anticipates due to the strong lattice potential this will tend to lock in at commensurate

[27] Chubukov and Morr, 1995

densities forming exciton 'Mott insulators'. We will wire this in by taking also the exciton-exciton dipolar interaction into account that surely promotes such orderings. In principle there is the interesting possibility that all these orders may coexist microscopically forming an 'antiferromagnetic supersolid'.[28] We find that at least for the strongly coupled 'small' excitons assumed here this does not happen. The reason is interesting. We already alluded to the dynamical frustration associated with the exciton delocalizing in the antiferromagnetic spin background in section 4.2. At finite densities this turns into a tendency to just **phase separate on a macroscopic scale**, in zero density antiferromagnets, exciton Mott insulators and high density diamagnetic exciton superfluids. For now we notice quickly that the exciton dipole repulsion is actually long-ranged,[29] instead of just the nearest neighbor repulsion discussed in this chapter. This simplification rules out the occurrence of frustrated phase separation as suggested for the electronic order in cuprates.[30] The influence of the long-range nature of the dipolar interaction is discussed in chapter 6.

[28] Zaanen, 1999

[29] Rademaker et al., 2013d

[30] Zaanen and Gunnarsson, 1989; Emery and Kivelson, 1993; Löw et al., 1994; Tranquada et al., 1995; and Zhang and Henley, 2003

It is disappointing that apparently in this system only conventional ground states occur. However, this is actually to a degree deceptive. The Hamiltonian describing the physics at the lattice scale describes a physics where the exciton- and spin motions are **entangled**: the way in which these subsystems communicate gets beyond the notion of just being strongly coupled, since the motions of the exciton motions and the spin dynamics cannot be separated. By coarse graining this all the way to the static order parameters (the mean fields) an effective disentanglement eventually results as demonstrated by the product ground states. However, upon going "off-shell" this spin-exciton entanglement becomes directly manifest in the form of unexpected and rather counterintuitive effects on the excitation spectrum. A simple example is the zero exciton density antiferromagnet. From the relatively thorough LSW-SCBA treatment of the one exciton problem[31] we already know that the resulting exciton spectrum can be completely different from that in a simple semiconductor. In this section we compute the linearized excitations around the pure antiferromagnet, recovering the LSW-SCBA result in the adiabatic limit where the exciton hopping is small compared to the exchange energy of the spin system, which leads to a strong enhancement of the exciton mass. In the opposite limit of fast excitons, the energy

[31] See section 4.2.

scale is recovered but the Ising confinement ladder spectrum revealed by the LSW-SCBA treatment is absent. The reason clear: in the language of this section, the couplings between the exciton- and spin-wave modes become very large and these 'spin wave interactions' need to be resummed in order to arrive at an accurate description of the exciton propagator.

The real novelty in this regard is revealed in the high density **exciton superfluid phase**. As shown in the previous section, by measuring the spin fluctuations one can in principle determine whether the excitons are condensed in a superfluid.

As a reminder let us recall our point of departure: the Hamiltonian describing strongly bound excitons propagating through a bilayer Heisenberg spin $1/2$ system. This model is derived at length in section 4.1 and here we just summarize the outcome. Due to the strong electron-electron interactions the electronic degrees of freedom are reduced to spin operators $\mathbf{s}_{il}$ governed by the bilayer Heisenberg model[32]

[32] Manousakis, 1991; and Chubukov and Morr, 1995

$$H_J = J \sum_{\langle ij \rangle, l} \mathbf{s}_{il} \cdot \mathbf{s}_{jl} + J_\perp \sum_i \mathbf{s}_{i1} \cdot \mathbf{s}_{i2}. \tag{5.12}$$

The subscript denotes spin operators on site i in layer $l = 1, 2$. The Heisenberg H_J is antiferromagnetic with $J > 0$ and $J_\perp > 0$. The interlayer exciton can hop around, thereby interchanging places with the spin background. In the strong-coupling limit of exciton binding energies the exciton hopping process is described by the Hamiltonian

$$H_t = -t \sum_{\langle ij \rangle} |E_j\rangle \left(|0\ 0\rangle_i \langle 0\ 0|_j + \sum_m |1\ m\rangle_i \langle 1\ m|_j \right) \langle E_i|. \tag{5.13}$$

where $|E\rangle$ is the exciton state on an interlayer rung, and $|s\ m\rangle$ represent the rung spin states. Whenever an exciton hops, it effectively exchanges the spin configuration on its neighboring site. In order to study the system with a finite density of excitons, we need to enrich the $t - J$ model with two extra terms: a chemical potential and an exciton-exciton interaction.

The **chemical potential** is given by

$$H_\mu = -\mu \sum_i |E_i\rangle \langle E_i| \tag{5.14}$$

which is a rather trivial statement. The exciton-exciton interaction requires some more thought. The bare interaction between two

interlayer excitons results from their electric dipole moment. Since all interlayer exciton dipole moments are pointing in the same direction the full exciton-exciton interaction is described by a repulsive $1/r^3$ interaction. The interaction strength decays so fast that we consider it reasonable to only include the nearest-neighbor repulsion,

$$H_{V_I} = V_I \sum_{\langle ij \rangle} \left(|E_i\rangle\langle E_i|\right)\left(|E_j\rangle\langle E_j|\right). \tag{5.15}$$

Note that especially in the region where we expect phase separation, the long-range nature of the dipolar interaction will become relevant.[33] For now we set V_I to be the energy scale associated with **nearest neighbor exciton repulsion**. This number can get quite high: given a typical interlayer distance of 8 Å and an intersite distance of 4 Å[34] the bare dipole interaction energy is 14 eV. In reality, we expect this energy to be lower due to quantum corrections and screening effects. However, the exciton-exciton interaction scale remains on the order of electronvolts and thus larger than the estimated Heisenberg J and hopping t.

[33] See chapter 6 for the influence of long-range interactions.

[34] Imada et al., 1998

We must pause here for a while and reflect on the possibility of interlayer hopping of electrons, which leads to the **annihilation of excitons**,

$$H_{t_\perp} = -t_\perp \sum_i |E_i\rangle\langle 0\ 0|_i + h.c. \tag{5.16}$$

This term explicitly breaks the $U(1)$ symmetry, which is associated with the conservation of excitons. While this term is almost certainly present in any realistic system, it is a matter of numbers whether it is relevant. In the present case the interlayer tunneling can be incorporated using perturbation theory in a renormalisation of the chemical potential μ. As a consequence we do not need to include the $t_\perp$ term in our model Hamiltonian.

The full model Hamiltonian describing a finite density of excitons in a strongly correlated bilayer is thus

$$H = H_J + H_t + H_\mu + H_{V_I}. \tag{5.17}$$

5.2.1 *Symmetries and an effective XXZ model*

The Hamiltonian (5.17) has five model parameters: J, $J_\perp$, t, V_I and μ. However, most properties of the excitons can be understood by considering the simpler problem of hard-core bosons on a

lattice. In this subsection we will argue that the exciton degrees of freedom can be described by an **effective** XXZ **model**.

Before characterizing different phases of the model we need to assess the **algebraic structure of the exciton** $t-J$ **model**. The set of all operators that act on the local Hilbert space form the **dynamical algebra**, whereas the symmetries of the system are grouped together in the **symmetry algebra**.

To derive the dynamical algebra, it is instructive to start with the bilayer Heisenberg model which has, on each interlayer rung, a $SO(4) \cong SU(2) \times SU(2)$ dynamical algebra. Upon inclusion of the exciton hopping term we need more operators, since now the local Hilbert space on an interlayer rung is five-dimensional (four spin states and the exciton). Consider the spin-to-exciton operator $E^+_{sm} \equiv |E\rangle\langle s\ m|$ and its conjugate $E^-_{sm} = (E^+_{sm})^\dagger$. Their commutator reads

$$[E^+_{sm}, E^-_{sm}] = |E\rangle\langle E| - |s\ m\rangle\langle s\ m| \equiv 2E^z_{sm} \tag{5.18}$$

where we have introduced the operator E^z_{sm} to complete a $SU(2)$ algebraic structure. We could set up such a construction for each of the four spin states $|s\ m\rangle$. Under these definitions the exciton hopping term (5.13) can be rewritten in terms of an XY**-model** for each spin state,

$$\begin{aligned} H_t &= -t \sum_{<ij>,sm} \left(E^+_{sm,i} E^-_{sm,j} + E^-_{sm,i} E^+_{sm,j} \right) && (5.19) \\ &= -2t \sum_{<ij>,sm} \left(E^x_{sm,i} E^x_{sm,j} + E^y_{sm,i} E^y_{sm,j} \right) && (5.20) \end{aligned}$$

where the sum over sm runs over the singlet and the three triplets. Note that the exciton chemical potential (5.14) acts as an externally applied magnetic field to this XY-model, and that the exciton-exciton repulsion (5.15) can be rewritten as an antiferromagnetic Ising term in the E^z_{sm} operators. The dynamical algebra therefore contains four $SU(2)$ algebras in addition to the $SO(4)$ from the bilayer Heisenberg part. The closure of such algebra is necessarily $SU(5)$, which is the largest algebra possible acting on the five-dimensional Hilbert space. Hence we need a full $SU(5)$ dynamical algebra to describe the exciton $t-J$ model at finite density.

From the XY-representation of the hopping term one can already deduce that we have four distinct $U(1)$ symmetries associated with spin-exciton exchange. The bilayer Heisenberg model

contains two separate $SU(2)$ symmetries, associated with in-phase and out-phase interlayer magnetic order. Therefore the **full symmetry algebra of the model is** $[SU(2)]^2 \times [U(1)]^4$.

Breaking of the $SU(2)$ symmetry amounts to magnetic ordering, which is most likely antiferromagnetic (and therefore also amounts to a breaking of the lattice symmetry). Each of the $U(1)$ algebras can be broken leading to exciton condensation. Note that next to possible broken continuous symmetries, there also might exist phases with broken translation symmetry. The checkerboard phase is an example of a phase where the lattice symmetry is broken into two sublattices.

Above we showed that the exciton hopping terms are similar to an XY-model. The main reason is that the excitons are, in fact, **hard-core bosons** and thus allow for a mapping onto pseudospin degrees of freedom. Viewed as such, the exciton-exciton interaction (5.15) is similar to an antiferromagnetic Ising term and the exciton chemical potential (5.14) amounts to an external magnetic field in the z-direction. Together they form an XXZ**-model with external field**, which has been investigated in quite some detail before[35] as well as in the context of exciton dynamics in cold atom gases.[36]

[35] Néel, 1936; Fisher and Nelson, 1974; Landau and Binder, 1981; van Otterlo et al., 1995; Kohno and Takahashi, 1997; and Yunoki, 2002

[36] Kantian et al., 2007

In order to understand the basic competition between the checkerboard phase and the superfluid phase of the excitons, it is worthwhile to neglect the magnetic degrees of freedom and study first this effective XXZ-model for the excitons only. In this context the transition between the checkerboard and superfluid phases is known as the **'spin flop'-transition**.[37] Whilst remembering that the exciton degrees of freedom are mapped onto the XXZ pseudospin degrees of freedom, we now quickly review the basics of the XXZ Hamiltonian

[37] Néel, 1936

$$H = -t \sum_{\langle ij \rangle} \left(E_i^x E_j^x + E_i^y E_j^y \right) - \mu \sum_i E_i^z + V_I \sum_{\langle ij \rangle} E_i^z E_j^z \qquad (5.21)$$

where $E^+ = |1\rangle\langle 0| = E^x + iE^y$ creates a hard-core bosonic particle $|1\rangle$ out of the vacuum $|0\rangle$. This model has a built-in competition between $t > 0$, which favors a superfluid state, and $V_I > 0$, which favors a solid state where all particles are on one sublattice and the other sublattice is empty. The external field or chemical potential μ tunes the total particle density. The ground state can now be found using mean field theory. It is known that for pseudospin

$S = \frac{1}{2}$ models in $(2+1)$d the quantum fluctuations are not strong enough to defeat classical order, therefore we can rely on mean field theory which is indeed supported by exact diagonalization studies.[38]

[38] Kohno and Takahashi, 1997

To find the ground state we introduce a **variational wavefunction** describing a condensate of excitons,

$$|\Psi\rangle = \prod_i \left(\cos\theta_i e^{i\psi_i}|1\rangle_i + \sin\theta_i|0\rangle_i\right). \tag{5.22}$$

The mean-field approximation amounts to choosing ψ_i constant and θ_i only differing between the two sublattices. We find the following mean-field energy

$$\begin{aligned} E/N &= -\frac{1}{8}tz\sin 2\theta_A \sin 2\theta_B + \frac{1}{8}V_I z\cos 2\theta_A \cos 2\theta_B \\ &\quad -\frac{1}{4}\mu\left(\cos 2\theta_A + \cos 2\theta_B\right). \end{aligned} \tag{5.23}$$

Let's rewrite this in terms of $\bar{\theta} = \theta_A + \theta_B$ and $\Delta\theta = \theta_A - \theta_B$,

$$\begin{aligned} E/N &= \frac{z}{8}\left((V_I - t)\cos^2\Delta\theta + (V_I + t)\cos^2\bar{\theta}\right) \\ &\quad -\frac{1}{2}\mu\cos\Delta\theta\cos\bar{\theta} - \frac{V_I z}{8}. \end{aligned} \tag{5.24}$$

When $|\mu| \geq \frac{1}{2}(V_I z + zt)$ the ground state is fully polarized in the z-direction. This means either zero particle density for negative μ, or a $\rho = 1$ for the positive μ case. Starting from the empty side, increasing μ introduces a smooth distribution of particles. This phase amounts to the superfluid phase of the excitons. The particle density on the two sublattices is equal and the total density is given by

$$\rho = \cos^2\theta = \frac{1}{2}\left(\cos\bar{\theta} + 1\right) = \frac{1}{2}\left(\frac{2\mu}{V_I z + zt} + 1\right). \tag{5.25}$$

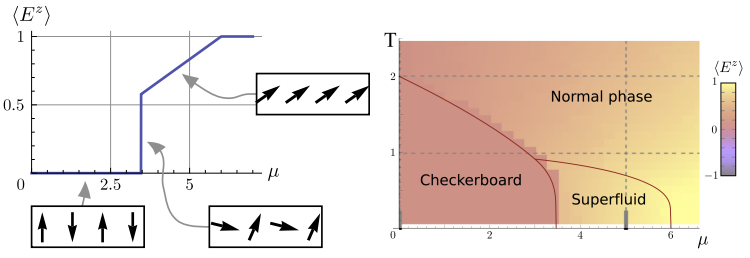

Figure 5.3: **Left:** The ground state phase diagram of the XXZ model (5.21). The graph shows the mean field particle density $\langle E^z\rangle$ as a function of μ, with model parameters $t = 1$ and $V_I = 2t$. One clearly distinguishes the fully polarized phases for large μ, the superfluid phase with a linear $\langle E^z\rangle$ vs μ dependence and the checkerboard phase with $\langle E^z\rangle = 0$. In between the checkerboard and the superfluid phase a non-trivial first order transition exists, with a variety of coexistence ground states with the same ground state energy. The insets show how the (E^x, E^z)-vectors look like in the different phases. **Right:** Finite temperature phase diagram of the XXZ model with the same parameters. The background coloring corresponds to a semi-classical Monte Carlo computation of $\langle E^z\rangle$, the solid lines are analytical mean field results for the phase boundaries. We indeed see the checkerboard phase and the superfluid phase, as well as a high-temperature non-ordered 'normal' phase.

At the critical value of the chemical potential given by

$$(\mu_c)^2 = \left(\frac{1}{2}z\right)^2 (V_I - t)(V_I + t). \tag{5.26}$$

a first order transition occurs towards the checkerboard phase: the spin flop transition. In the resulting phase, which goes under various names such as the antiferromagnetic,[39] solid, checkerboard or Wigner crystalline phase, the sublattice symmetry is broken. The resulting ground state phase diagram is shown in figure 5.3, where a graph of the particle density as a function of μ is given.

At **finite temperatures** in $(2+1)$d there can be algebraic long-range order. At some critical temperature a Kosterlitz-Thouless phase transition[40] will destroy this long-range order. The topology of the phase diagram, however, can be obtained using the finite temperature mean field theory for which we need to minimize the mean field thermodynamic potential[41]

$$\begin{aligned}\Phi/N &= -kT\log\left(2\cosh\left(\frac{\beta m}{2}\right)\right) + \frac{1}{2}m\tanh\left(\frac{\beta m}{2}\right) \\ &\quad + \frac{z}{8}\tanh^2\left(\frac{\beta m}{2}\right) \\ &\quad \times \left[(V_I - t)\cos^2\Delta\theta + (V_I + t)\cos^2\bar{\theta} - V_I\right] \\ &\quad - \frac{\mu}{2}\tanh\left(\frac{\beta m}{2}\right)\cos\Delta\theta\cos\bar{\theta}.\end{aligned} \tag{5.27}$$

Expectation values are now given in the form of

$$\langle S^x_{i\in A}\rangle = \frac{1}{2}\sin 2\theta_A \tanh\left(\frac{\beta m}{2}\right), \tag{5.28}$$

and the parameter m needs to be determined self-consistently. The resulting phase diagram is shown in figure 5.3, right, which is of the form discussed by Fisher and Nelson, 1974.

The **first order quantum critical point** at μ_c turns out to be non-trivial, a point which is usually overlooked in the literature. A trivial first order transition occurs when there are two distinct phases with exactly the same energy. In the case presented here, there is a infinite set of mean field order parameters all yielding different phases yet still having the same energy. A simple analytic calculation shows that the energy of the ground state at the critical point is $E_c = -V_I z/8$. Now rewrite the mean field parameters ρ_A

[39] If we associate the presence of a particle with spin up, and the absence with spin down, then the solid phase is identified with an Ising antiferromagnet. However, one should not confuse this with the *actual* antiferromagnetism present in the spin sector of the full exciton $t-J$ model. To avoid confusion, from now on we will use the term 'antiferromagnetism' only when referring to the spin degrees of freedom in the full exciton $t-J$ model.

[40] Kosterlitz and Thouless, 1973

[41] Yeomans, 1992

and ρ_B into a sum and difference parameter

$$\rho = \frac{1}{2}(\rho_A + \rho_B), \tag{5.29}$$

$$\Delta_\rho = \frac{1}{2}(\rho_A - \rho_B). \tag{5.30}$$

For each value of Δ_ρ with $|\Delta_\rho| \leq (1/2)$ we can find a value of ρ such that the mean field energy is exactly $-V_I z/8$.

This has interesting consequences. If one can control the density instead of the chemical potential around a first order transition, in general phase separation would occur between the two competing phases. From the mean field considerations above it is unclear what would happen in a system described by the XXZ Hamiltonian (5.21). All phases would be equally stable, at least from an energy perspective, and every phase may occur in regions of any size. Such a highly degenerate state may be very sensible to small perturbations. We consider it an interesting open problem to study the dynamics of such a highly degenerate system, and whether this degeneracy may survive the inclusion of quantum corrections.

Note that qualitatively a possible $t_\perp$ term is irrelevant, which can be seen in the XXZ pseudospin language where it takes the form of a tilt of the magnetic field in the x-direction,

$$H_{t_\perp} = -t_\perp \sum_i E_i^x. \tag{5.31}$$

5.2.2 *Ground state phase diagram: variational wavefunction*

In the previous section we have seen that the effective XXZ model predicts the existence of both a exciton **superfluid phase** and a **checkerboard phase**, separated by a first order transition. Further extending these results yields the ground state phase diagram for the full exciton $t - J$ model (5.17).

We will proceed along the same lines as in the previous section. Hence we need a **variational wavefunction**, which we simulate numerically to obtain an unbiased view on the possible ground state phases. Based on the numerical results we apply mean field theory, which is very reliable due to the hard-core bosonic nature of excitons. The analytical mean field also allows us to characterize the three distinct phases: the **antiferromagnet**, the **superfluid** and the **checkerboard**. Finally, combining the numerical results and

the analytical mean field results we obtain the ground state phase diagram in figure 5.8.

Recall that the local Hilbert space consists of four spin states $|s\ m\rangle$ and the exciton state $|E\rangle$. We therefore propose a variational wavefunction consisting of a product state of superpositions all five states on each rung. For the spin states we take the $SO(4)$ **coherent state**[42]

[42] van Duin, 1999

$$\begin{aligned} |\Omega_i\rangle &= -\frac{1}{\sqrt{2}}\sin\chi_i \sin\theta_i e^{-i\phi_i}|1\ 1\rangle_i \\ &\quad +\frac{1}{\sqrt{2}}\sin\chi_i \sin\theta_i e^{i\phi_i}|1\ -1\rangle_i \\ &\quad +\sin\chi_i\cos\theta_i|1\ 0\rangle_i - \cos\chi_i|0\ 0\rangle_i \end{aligned} \tag{5.32}$$

which needs to be superposed with the exciton state,

$$|\Psi_i\rangle = \sqrt{\rho_i}e^{i\psi_i}|E_i\rangle + \sqrt{1-\rho_i}|\Omega_i\rangle \tag{5.33}$$

to obtain the total variational wavefunction

$$|\Psi\rangle = \prod_i |\Psi_i\rangle. \tag{5.34}$$

Given this wavefunction, the expectation value of a product of operators on different sites decouples, $\langle A_i B_j\rangle = \langle A_i\rangle\langle B_j\rangle$. The only nonzero expectation values of spin operators are for $\widetilde{\mathbf{S}}_i = \mathbf{s}_{i1} - \mathbf{s}_{i2}$ and it equals

$$\langle\Omega_i|\widetilde{\mathbf{S}}_i|\Omega_i\rangle = \sin 2\chi_i \begin{pmatrix} \sin\theta_i\cos\phi_i \\ \sin\theta_i\sin\phi_i \\ \cos\theta_i \end{pmatrix} = \sin 2\chi_i\ \hat{\mathbf{n}}_i \tag{5.35}$$

where $\hat{\mathbf{n}}_i$ is the unit vector described by the angles θ and ϕ. This variational wavefunction therefore assumes interlayer Néel order of magnitude $\sin 2\chi_i$, which enables us to correctly interpolate between the perfect Néel order at $\chi = \pi/4$ and the singlet phase $\chi = 0$ present in the bilayer Heisenberg model. The exciton density at a rung i is trivially given by ρ_i.

Given the variational wavefunction, we can use **simulated annealing** to develop an unbiased view on the possible ground state phases. Therefore we start out with a lattice, on each lattice site the variables θ_i, χ_i, ϕ_i, ψ_i and ρ_i and with periodic boundary

conditions. The energy of a configuration is

$$\begin{aligned} E &= \frac{1}{2}J \sum_{<ij>} (1-\rho_i)(1-\rho_j) \sin 2\chi_i \sin 2\chi_j \, \hat{n}_i \cdot \hat{n}_j \\ &\quad -J_\perp \sum_i (1-\rho_i)\cos^2\chi_i - \mu \sum_i \rho_i + V_I \sum_{<ij>} \rho_i \rho_j \\ &\quad -\frac{1}{2}t \sum_{<ij>} \sqrt{\rho_i(1-\rho_i)\rho_j(1-\rho_j)}\cos(\psi_i - \psi_j) \\ &\quad \times \left(\cos\chi_i \cos\chi_j + \sin\chi_i \sin\chi_j \, \hat{n}_i \cdot \hat{n}_j\right) \end{aligned} \tag{5.36}$$

[43] See section 3.3 for a detailed description of Monte Carlo techniques.

We performed standard **Metropolis Monte Carlo updates**[43] of the lattice with fixed total exciton density. The fixed total exciton density is ensured as follows: if during an update the exciton density ρ_i is changed, the exciton density on one of the neighboring sites is corrected such that the total exciton density remains constant.

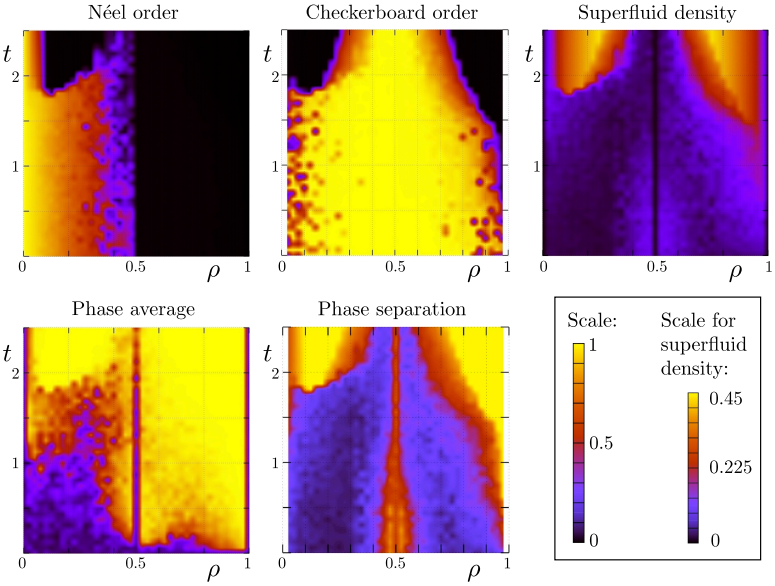

Figure 5.4: Results from the semi-classical Monte Carlo simulations. Here shown are color plots, with on the horizontal axes the exciton density ρ and on the vertical axes the hopping parameter t (in eV). Other parameters are fixed at $J = 125$ meV, $\alpha = 0.04$ and $V_I = 2$ eV. The five measurements shown here are the Néel order parameter (5.37), the checkerboard order parameter (5.38), the superfluid density (5.39), the phase coherence (5.40), and the ratio signaling phase separation according to equation (5.42), 0 means complete phase separation, 1 means no phase separation. Notice that the prominent line at $\rho = 0.5$ signals the checkerboard phase.

The main results of the simulation are shown in figure 5.4, for various values of the hopping parameter t and exciton density ρ. We performed the computations on a 10×10 lattice. Notice that even though true long-range order does not exist in two dimensions, the range of possible ordered phases is longer than the size of our simulated lattice. The other parameters are fixed at

$J = 125$ meV, $\alpha = 0.04$ and $V_I = 2$ eV. The Heisenberg couplings $J = 125$ meV and $\alpha = 0.04$ are obtained from measurements of undoped YBCO-samples,[44] which we consider to be qualitatively indicative of all strongly correlated electron bilayers. The dipolar coupling is estimated at 2 eV, following our discussion in the introduction.

[44] Imada et al., 1998; and Tranquada et al., 1989

For each value of ρ and t we started at relatively high temperatures $T = 0.1$ eV and then slowly reducing the temperature to 10^{-5} eV while performing a full update of the whole lattice 10 million times. We expect that by such a slow annealing we obtain the true ground state of (5.36) without any topological defects or false vacua. Once arrived at the low temperature state, we performed measurements over 200.000 full updates of the system.

We measured six different parameters of interest:

- The **Néel order** parameter defined by

$$\text{Neel} = \left|\left| \frac{1}{N} \sum_i (-1)^i (1-\rho_i) \sin 2\chi_i \hat{\mathbf{n}}_i \right|\right| \tag{5.37}$$

  where we first sum over all spin vectors and then take the norm.

- The **checkerboard order**, defined as the difference in exciton density between the sublattices divided by the maximal difference possible. The maximal difference possible equals $\text{Min}(\overline{\rho}, 1-\overline{\rho})$, so

$$\text{Checkerboard} = \frac{\frac{1}{N}\sum_i (-1)^i \rho_i}{\text{Min}(\overline{\rho}, 1-\overline{\rho})}. \tag{5.38}$$

- The **superfluid density** is given by the expectation value of the exciton operator. Here we don't make a distinction between singlet exciton condensation or triplet exciton condensation. Therefore

$$\text{Superfluid density} = \frac{1}{N} \sum_i \sqrt{\rho_i (1-\rho_i)}. \tag{5.39}$$

- Now the superfluid density is not the only measure of the condensate, we can also probe the **rigidity of the phase** ψ. Therefore we sum up all the phase factors on all sites,

$$\text{Phase average} = \left| \frac{1}{N} \sum_i e^{i\psi_i} \right|. \tag{5.40}$$

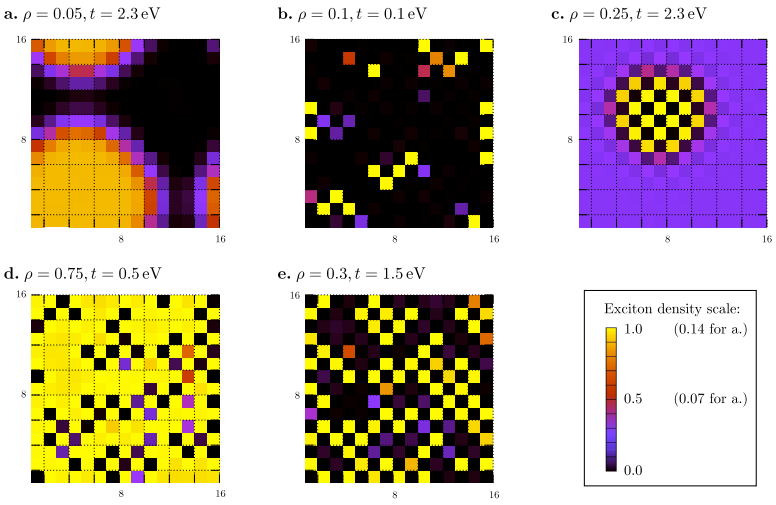

Figure 5.5: Typical configurations for the exciton density per site, obtained in the Monte Carlo simulation on a 16×16 square lattice. The color scale indicates the exciton density. All five figures have model parameters $J = 125$ meV, $\alpha = 0.04$ and $V_I = 2$ eV. **a:** Separation between the antiferromagnetic phase (without excitons, hence shown black) and the exciton condensate with smooth exciton density ($\rho = 0.05$, $t = 2.3$ eV). **b:** Separation between checkerboard-like localized excitons and an antiferromagnetic background ($\rho = 0.1$, $t = 0.1$ eV). **c:** Separation between the checkerboard phase and a low density exciton condensate ($\rho = 0.25$, $t = 2.3$ eV). **d:** Separation between the checkerboard phase and a high density exciton condensate ($\rho = 0.75$, $t = 0.5$ eV). **e:** The region where antiferromagnetic order, checkerboard order and the exciton condensate are all present ($\rho = 0.3$, $t = 1.5$).

If the phase is disordered, this sum tends to zero. On the other hand, complete phase coherence in the condensate phase implies that this quantity equals one.

- Finally, we considered a measure of **phase separation** between the checkerboard phase and the superfluid phase. If the exciton condensate and the checkerboard phase are truly coexisting, then the maximal superfluid density attainable would be

$$\begin{aligned}\text{Max SF density} = &\frac{1}{2}\sqrt{(\overline{\rho}+\Delta_\rho)(1-\overline{\rho}-\Delta_\rho)} \\ &-\frac{1}{2}\sqrt{(\overline{\rho}-\Delta_\rho)(1-\overline{\rho}+\Delta_\rho)}\end{aligned} \tag{5.41}$$

where $\Delta_\rho = \frac{1}{N}\sum_i (-1)^i \rho_i$. If there is phase separation, however, the actual superfluid density is less than this maximal density. Therefore we also measured the ratio

$$\text{Ratio} = \frac{\text{Superfluid density}}{\text{Max SF density}} \tag{5.42}$$

to quantify the extent of phase separation. Now if this ratio is less than 1, we have phase separation.

The results for a full scan for the range $0 < \rho < 1$ and $0 < t < 2.5$ eV are shown in figure 5.4. In figures 5.5 and 5.6 we have displayed typical exciton density configurations for various points in the phase diagram. These results combined suggest

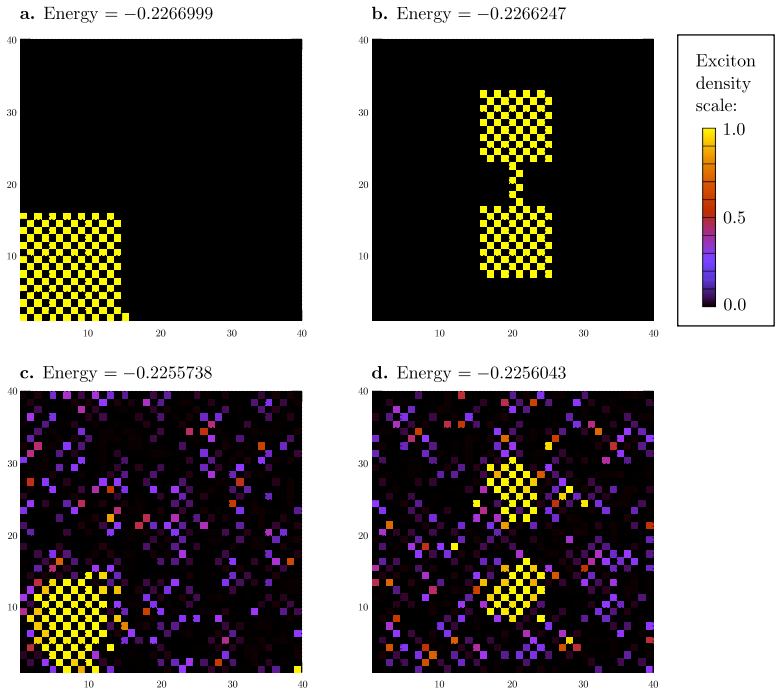

Figure 5.6: Different exciton configurations with their respective energies on a 40×40 lattice, to show whether there is macroscopic phase separation. The model parameters are $t = 0.5$ eV, $J = 125$ meV, $\alpha = 0.04$, $V_I = 2$ eV and $\rho = 0.06625$. Yellow indicates the presence of excitons, and in the black regions there is antiferromagnetic order. **a:** The lowest energy state is the one with complete macroscopic phase separation. **b:** More complicated phase separation, such as the halter form depicted here, are higher in energy. **c:** Starting at high temperatures with the configuration a, we slowly lowered the temperature. The resulting configuration shown here is a local minimum. **d:** Using the same slow annealing as for c starting from configuration b. The local energy minimum obtained this way is lower in energy than the configuration c. We conclude that even though macroscopic phase separation has the lowest energy, there are many local energy minima without macroscopic phase separation.

that there are **three main phases** present in the system: the antiferromagnet at low exciton densities, the exciton superfluid at high exciton hopping energies and the checkerboard around half-filling. For most parts of the phase diagram, however, the competition between the three phases results in phase separation.

Let us investigate the **phase separation** in somewhat more detail. In section 4.2 we found that the motion of an exciton in an antiferromagnetic background leads to dynamical frustration. In other words: excitons do not want to be together with antiferromagnetism. The introduction of a finite density of excitons will therefore induce phase separation. For large t, we find macroscopic phase separation between the antiferromagnet and the exciton superfluid, see figure 5.5a. At low exciton kinetic energy the excitons will be localized in a checkerboard pattern as can be seen in figure 5.5b.

Close to half-filling the role of the dipole repulsion V_I becomes increasingly relevant. The first order 'spin flop' transition implies that there will be phase separation between the superfluid and the

checkerboard order. Figures 5.5c and d show this phase separation. Finally there is a regime where the condensate, the checkerboard order and the Néel order are all present. However, given the dynamical frustration at one hand and the spin-flop transition at the other hand, we again predict phase separation. A typical exciton configuration is shown in figure 5.5e.

Phase separation is thus widespread, based on results obtained by slow annealing starting at high temperatures. However, annealing can lead to the freezing in of defects, which prevents us from reaching the true ground state. In order to investigate whether we have **frustrated or macroscopic phase separation**, we construct custom-made phase separated configurations and compare their energies in figure 5.6. The lowest energy configuration (5.6a) has macroscopic phase separation between the checkerboard and the antiferromagnetic phase. Intermediate states with one blob of excitons (5.6c) are slightly higher in energy than states with two blobs of excitons (5.6d). However, even though macroscopic phase separation has the lowest energy, configurations with more blobs have more entropy. Consequently for any nonzero temperatures complete macroscopic phase separation is not the most favorable option. This is indeed picked up by the numerical simulations: annealing leads to high-entropy states such as figure 5.6d rather than to the lowest energy configuration.

We thus conclude that the dominant phases are the antiferromagnet, the superfluid and the checkerboard. The competition between these three phases leads to phase separation in most parts of the phase diagram. The unbiased Monte Carlo simulations shows the direction in which further analytical research should be directed: we will use mean field theory to characterize the three phases more thoroughly.

5.2.3 Mean field theory and characterization of the phases

Given the fact that we are dealing with a hard-core boson problem, we know that **mean field theory is qualitatively correct**. The only open issue is whether one can tune the exciton chemical potential rather than the exciton density in realistic experiments. Since we are prescient about the many first-order phase transitions present, we will perform the analysis with a fixed exciton density (the canonical ensemble). A transformation back to the grand-canonical

ensemble can be made given the explicit μ vs. ρ relations.

Now the numerical simulations suggest that the mean field parameters only need to depend on the sublattice,

$$\rho_i = \begin{cases} \rho_A & i \in A \\ \rho_B & i \in B \end{cases} \tag{5.43}$$

and so forth for χ, θ, ψ and ϕ. With this **broken translational symmetry** we anticipate the antiferromagnetic and checkerboard order. Evaluation of the energy $E = \langle \Psi | H | \Psi \rangle$ under the variational wavefunction directly suggests that we can set $\theta = \psi = \phi = 0$ on all sites.[45] We are left with four parameters ρ_A, ρ_B, χ_A and χ_B, and as it turns out it will be more instructive to rewrite these in terms of sum and difference variables,

$$\overline{\rho} = \frac{1}{2}(\rho_A + \rho_B) \tag{5.44}$$

$$\Delta_\rho = \frac{1}{2}(\rho_A - \rho_B) \tag{5.45}$$

$$\overline{\chi} = \chi_A + \chi_B \tag{5.46}$$

$$\Delta_\chi = \chi_A - \chi_B \tag{5.47}$$

[45] By setting $\theta = \phi = 0$ we restrict the spin vectors to be pointing in the $\pm z$ direction only. Since we anticipate magnetic ordering we have the freedom to choose the direction of the ordering. Similar arguments hold for the choice $\psi = 0$; when breaking the $U(1)$ symmetry associated with exciton condensation we are free to choose the phase direction.

The mean field energy per site is now given by

$$\begin{aligned} E/N = & \frac{1}{8} Jz \left((1-\overline{\rho})^2 - \Delta_\rho^2 \right) (\cos 2\Delta_\chi - \cos 2\overline{\chi}) \\ & - \frac{1}{2} J_\perp \left[(1-\overline{\rho})(\cos\overline{\chi}\cos\Delta_\chi + 1) + \Delta_\rho \sin\overline{\chi}\sin\Delta_\chi \right] \\ & - \frac{1}{4} zt \sqrt{((1-\overline{\rho})^2 - \Delta_\rho^2)(\overline{\rho}^2 - \Delta_\rho^2)}\cos\Delta_\chi \\ & - \mu\overline{\rho} + \frac{1}{2} zV_I(\overline{\rho}^2 - \Delta_\rho^2). \end{aligned} \tag{5.48}$$

which needs to be minimized for a fixed average exciton density $\overline{\rho}$ with the constraint $|\Delta_\rho| \leq \min(\overline{\rho}, 1-\overline{\rho})$. The resulting mean field phase diagram for typical values of $J, J_\perp$ and V_I, for various $t, \overline{\rho}$, is shown in figure 5.7.

As long as the exciton density is set to zero, the mean field ground state is given by the same ground state as for the bilayer Heisenberg model. That is the **antiferromagnetic phase** parametrized by

$$\rho = 0,\ \overline{\chi} = 0 \text{ and } \cos\Delta_\chi = \frac{J_\perp}{Jz} \equiv \alpha. \tag{5.49}$$

The Néel order is given by

$$\frac{1}{N}\sum_i (-1)^i \langle \widetilde{S}_i^z \rangle = \sqrt{1-\alpha^2} \tag{5.50}$$

and the energy of the antiferromagnetic state is

$$E = -\frac{1}{4} Jz(1+\alpha)^2. \tag{5.51}$$

The introduction of excitons in an antiferromagnetic background leads to dynamical frustration effects which disfavors the coexistence of excitons and antiferromagnetic order.[46] In fact, the numerical simulations already ruled out coexistence of superfluidity and antiferromagnetism.

[46] See section 4.2.

For large exciton hopping energy t it becomes more favorable to mix delocalized excitons into the ground state. Due to the bosonic nature of the problem this automatically leads to **exciton condensation**. The delocalized excitons completely destroy the antiferromagnetic order and the exciton condensate is described by a superposition of excitons and a singlet background,

$$|\Psi\rangle = \prod_i \left(\sqrt{\rho}|E_i\rangle + \sqrt{1-\rho}|0\ 0\rangle_i \right). \tag{5.52}$$

Here we wish to emphasize the ubiquitous coupling to light of the superfluid. The dipole matrix element allows only zero spin transitions, and since the exciton itself is also $S = 0$ the dipole matrix element is directly related to the superfluid density,

$$\begin{aligned} \langle \sum_\sigma c_{i1\sigma}^\dagger c_{i2\sigma} \rangle &= \langle E| \left(c_{1\uparrow}^\dagger c_{2\uparrow} + c_{1\downarrow}^\dagger c_{2\downarrow} \right) |0\ 0\rangle \\ &= \frac{1}{\sqrt{2}} \sqrt{\rho(1-\rho)} \langle \uparrow\downarrow_1\ \ 0_2| \\ &\quad \left(c_{1\uparrow}^\dagger c_{2\uparrow} + c_{1\downarrow}^\dagger c_{2\downarrow} \right) (|\uparrow_1 \downarrow_2\rangle - |\downarrow_1 \uparrow_2\rangle) \\ &= \sqrt{2\rho(1-\rho)} \end{aligned} \tag{5.53}$$

The dipole matrix element thus acts as the order parameter associated with the superfluid phase. In most bilayer exciton condensates, such as the one in the quantum Hall regime,[47] this order parameter is also nonzero in the normal phase because of interlayer tunneling of electrons. One can therefore not speak strictly about spontaneous breaking of $U(1)$ symmetry in such systems;

[47] Eisenstein and MacDonald, 2004

there is already explicit symmetry breaking due to the interlayer tunneling. In strongly correlated electron systems the finite $t_\perp$ can be incorporated as a virtual process since the energy scales associated with the chemical potential are much larger than $t_\perp$. As discussed at the beginning of this section, the Mott insulating bilayers now effectively allow for spontaneous $U(1)$ symmetry breaking, and the above dipole matrix element acts as a true order parameter. Note that the irrelevance of interlayer hopping $t_\perp$ implies that this order parameter is, unfortunately, not reflected in photon emission or interlayer tunneling measurements.

The exciton condensate is in fact a standard **two-dimensional Bose condensate**. The $U(1)$ symmetry present in the XY-type exciton hopping terms is spontaneously broken and we expect a linearly dispersed Goldstone mode in the excitation spectrum, reflecting the rigidity of the condensate.

The energy of the singlet exciton condensate is

$$E = -J_\perp - \frac{(\mu + \frac{1}{4}zt - J_\perp)^2}{zt + 2V_I z} \tag{5.54}$$

and the exciton density is given by

$$\overline{\rho} = 2\frac{\mu + \frac{1}{4}zt - J_\perp}{zt + 2V_I z}. \tag{5.55}$$

Whenever the exciton hopping is small, the introduction of excitons into the system leads to the **'spin flop' transition towards the checkerboard phase**. As shown in the context of the XXZ model, this phase implies that one sublattice is completely filled with excitons and the other sublattice is completely empty. On the empty sublattice, any nonzero $J_\perp$ will guarantee that the singlet spin state has the lowest energy. Hence the average exciton density is here $\overline{\rho} = \Delta_\rho = 1/2$ and the energy of the checkerboard phase is given by

$$E = -\frac{1}{2}J_\perp - \frac{1}{2}\mu. \tag{5.56}$$

It is interesting to note that the checkerboard phase is in fact similar to a Bose Mott insulator: with the new doubled unit cell we have one exciton per unit cell. The nearest neighbor dipole repulsion now acts as the 'on-site' energy preventing extra excitons per unit cell.

The mean field theory also predicts, for a small region with intermediate t and small exciton densities, the **coexistence of antiferromagnetism and the condensate**. This is, however, an artifact of the theory, since the numerical simulations show that here phase separation between the three different phases is favorable.

Finally, when the exciton density is 1 we have a system composed of excitons only. In the parlance of hard-core bosons this amounts to a **exciton Mott insulator**. This rather featureless phase is adiabatically connected to a standard electronic band insulator. Namely, the system is now composed of two layers where each layer has an even number of electrons per unit cell. The energy of the exciton Mott insulator is

$$E = -\mu + \frac{1}{2} V_I z. \tag{5.57}$$

In the mean field theory just described many **phase transitions** were first order, in the sense that the exciton density varies discontinuously along the transition. The critical values of t/J or μ along the second order transitions are

$$(t/J)_{c,\mathrm{AF}\to\mathrm{CO}} = \frac{2Jz(1+\alpha) - 4\mu}{J_\perp} \tag{5.58}$$

$$(t/J)_{c,\mathrm{EC}\to\mathrm{CO}} = 1 - \frac{2\mu}{Jz} + \sqrt{(1+8\alpha) + \left(\frac{2\mu}{Jz}\right)^2 - 4\left(3\frac{\mu}{Jz} - \frac{2V_I}{J}(1-\alpha)\right)} \tag{5.59}$$

$$\mu_{c,\mathrm{EC}\to\mathrm{EI}} = J_\perp + \frac{1}{4} zt + V_I z \tag{5.60}$$

and the critical values for the first order transitions are

$$\mu_{c,\mathrm{AF}\to\mathrm{CB}} = \frac{1}{2} Jz(1+\alpha^2) \tag{5.61}$$

$$\mu_{c,\mathrm{CB}\to\mathrm{EI}} = V_I z + J_\perp \tag{5.62}$$

$$(t/J)_{c,\mathrm{AF}\to\mathrm{EC}} = 2(1+\alpha^2) - 4\frac{\mu}{Jz} + 2\sqrt{(1-\alpha^2)\left(4\frac{\mu}{Jz} - (1+\alpha)^2 - 2\frac{V_I}{J}\right)} \tag{5.63}$$

$$(t/J)_{c,\mathrm{CB}\to\mathrm{EC}} = 4\sqrt{\left(\frac{\mu}{Jz} - \alpha\right)\left(\frac{V_I}{J} + \alpha - \frac{\mu}{Jz}\right)} \tag{5.64}$$

$$(t/J)_{c,\mathrm{CO}\to\mathrm{CB}} = \frac{2\alpha^2}{2\frac{\mu}{Jz} - 1} - 2\alpha + \sqrt{\left(1 - \frac{\alpha^2}{2\frac{\mu}{Jz} - 1}\right)\left(2\left(\frac{V_I}{J} + \alpha - \frac{\mu}{Jz}\right) - \frac{\alpha^2}{2\frac{\mu}{Jz} - 1}\right)}. \tag{5.65}$$

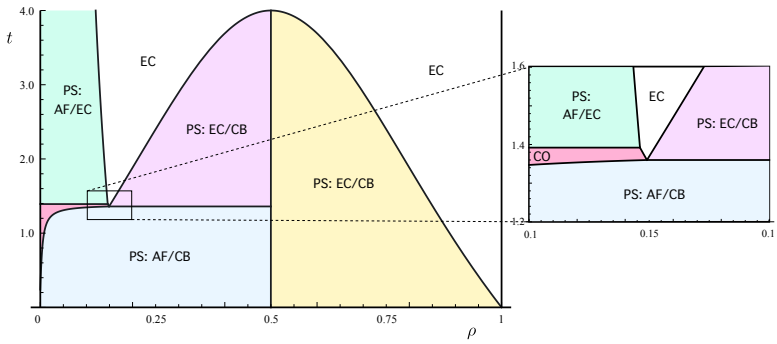

Figure 5.7: The canonical mean-field phase diagram for typical values of $J = 125$ meV, $\alpha = 0.04$ and $V_I = 2$ eV whilst varying t and the exciton density ρ. In the absence of exciton, at $\rho = 0$, we have the pure antiferromagnetic Néel phase (AF). Exactly at half-filling of excitons ($\rho = 1/2$) and small hoping energy $t < 2V_I$ we find the checkerboard phase (CB) where one sublattice is filled with excitons and the other sublattice is filled with singlets. For large values of t we find the singlet exciton condensate (EC), given by the wavefunction $\prod_i \left(\sqrt{\rho}\hat{E}^+_{00,i} + \sqrt{1-\rho}\right)|0\,0\rangle_i$. The coexistence of antiferromagnetism and superfluidity for small ρ and t is an artifact of the mean field theory. Conform the Monte Carlo results of figure 5.4, for most parts of the phase diagram phase separation (PS) is found. The analytical mean field theory incorrectly predicts coexistence of antiferromagnetism and superfluidity (CO).

Here the subscripts indicate the phases: antiferromagnetic phase (AF), coexistence phase (CO), exciton condensate (EC), exciton Mott insulator (EI), checkerboard phase (CB).

For any nonzero α the **first order transitions** from the antiferromagnetic or coexistence phase towards the checkerboard phase are 'standard' in the sense that at the critical value of μ there are only two mean field states with equal energy. This is also true for the transitions from the antiferromagnet to the exciton condensate except at a single point. At the tricritical point

$$t_c = 2J\sqrt{2V_I/J - 1} \tag{5.66}$$

$$\mu_c = J_\perp - \frac{1}{4}zt + \frac{1}{2}Jz(1-\alpha)\sqrt{2V_I/J + t/J} \tag{5.67}$$

separating the coexistence phase, the antiferromagnetic phase and the exciton condensate, we can set the parameters $\overline{\chi} = 0$, $\Delta_\rho = 0$ and Δ_χ given by the value in the coexistence phase. Now the energy becomes independent of the exciton density $\overline{\rho}$. Similarly, at the critical value of

$$\mu_c = J_\perp + \frac{1}{2}V_I z \pm \frac{1}{4}\sqrt{(2V_I z)^2 - (zt)^2} \tag{5.68}$$

describing the transition between the checkerboard phase to the singlet exciton condensate, we can choose the mean field parameters $\overline{\chi} = 0$, $\Delta_\chi = 0$ and

$$\Delta_\rho = \frac{1}{\sqrt{2}}\sqrt{(1 - 2\rho + 2\rho^2) - \frac{2V_I|1-2\rho|}{\sqrt{4V_I^2 - t^2}}}. \tag{5.69}$$

With these parameters, the energy becomes independent of ρ.

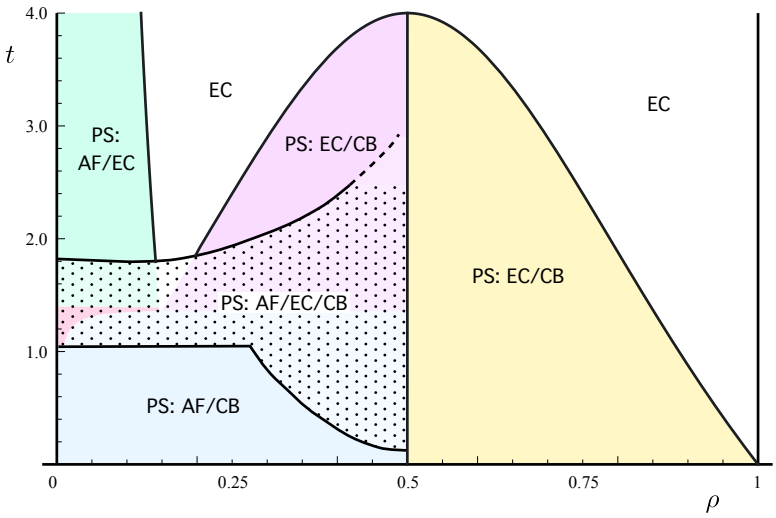

Figure 5.8: The canonical ground state phase diagram of the exciton $t-J$ model, which is a combination of the semi-classical Monte Carlo result and the mean field computations. In the background we have put the mean field phase diagram of figure 5.7, whilst the lines show the phase diagram as obtained from the Monte Carlo simulations. The dotted area represents phase separation between the condensate, antiferromagnetic and checkerboard order. Furthermore: EC means exciton condensate, CB means checkerboard phase, AF means antiferromagnetism and PS stands for phase separation.

This implies that the mean field theory predicts highly degenerate states at the critical values of μ, similar to the one we found in the XXZ model. The phase separation that thus occurs can be between an infinite set of possible ground states that have all a different exciton density. Coincidentally, the numerical simulations indicate that around the two 'degenerate' critical points indeed all the three phases are present. And whilst macroscopic phase separation has probably the lowest energy, the analysis of figure 5.6 suggests that more complicated patterns of phase separation are likely to occur. The degeneracy of the critical points in mean field theory might be responsible for the rich physics in this regions of the phase diagram.

We can **combine the unbiased numerical simulations** of figure 5.4 with the **analytical mean field results** of figure 5.7 to derive the **complete phase diagram of the exciton $t-J$ model** in figure 5.8. There are three main phases: the antiferromagnet at zero exciton density, the checkerboard at $\rho = 1/2$ and the superfluid at high hopping energy t. For most parts of the phase diagram, phase separation between these three phases occurs in any combination possible. The competition between these three phases leads in general to macroscopic phase separation.

Finally, within the limitations of the semi-classical Monte Carlo approach we can make a rough estimate of the **transition temper-**

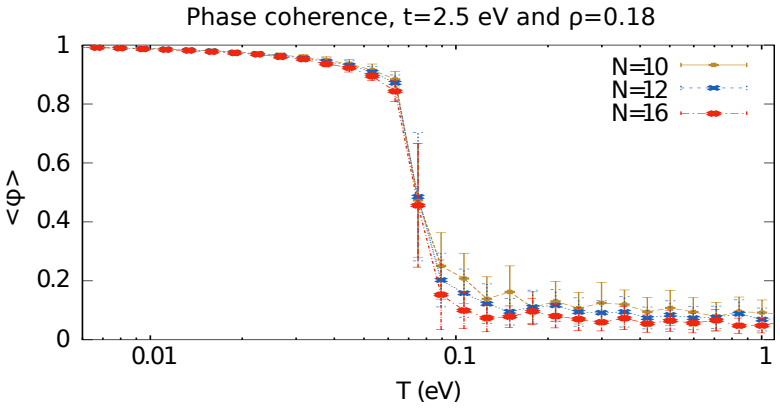

Figure 5.9: Finite temperature graph of the phase coherence in the exciton condensate region of the phase diagram. Here $t = 2.5$ eV and $\rho = 0.18$ and the other parameters are the same as in a. A clear transition is observed at around 0.06 eV, which amounts to a transition temperature of about 700 Kelvin.

ature towards the superfluid state. Given a typical point in the phase diagram where the exciton condensate exists, at $t = 2.5$ eV and $\rho = 0.18$, we find a Kosterlitz-Thouless transition temperature of approximately 700 Kelvin, see figure 5.4c. This number should be taken not too seriously, as the exciton $t - J$ model might not be applicable at such high temperatures given possible exciton dissociation. Additionally, at high temperatures the electron-phonon coupling becomes increasingly important which is something we neglect in our exciton $t - J$ model. Nonetheless, our estimate suggests that exciton superfluidity may extend to quite high finite temperatures.

5.2.4 *The Heisenberg equations of motion method*

In physical experiments one usually probes the **elementary excitations** of a phase. The dispersion of these excitations can be computed using the 'equations of motion'-method based on the work of Zubarev, 1960. The aim of this method is to find the spectrum of excitations, building on the foundations given by the mean field approximation. Let us now introduce this method, and subsequently use it to derive the excitations of the three phases of the exciton $t - J$ model.

Given a full set of local operators $\mathcal{A}_i^\ell$, we can construct the Heisenberg equations of motion

$$i\partial_t \mathcal{A}_i^\ell = [\mathcal{A}_i^\ell, H] \tag{5.70}$$

which is in general impossible to solve. We employ the notation

that i indicates the lattice site, and ℓ is the index denoting the type of operator. The right hand side of this equation contains products of operators at different lattice sites. Such **products can be decoupled** within the mean field approximation as [48]

[48] Zubarev, 1960; and Oles et al., 2000

$$\mathcal{A}_i^\ell \mathcal{A}_j^{\ell'} \to \langle \mathcal{A}_i^\ell \rangle \mathcal{A}_j^{\ell'} + \mathcal{A}_i^\ell \langle \mathcal{A}_j^{\ell'} \rangle \tag{5.71}$$

where i and j are different lattice sites. Upon Fourier transforming lattice position into momentum and time into energy, we thus obtain a set of linear equations for the operators,

$$\omega_q \mathcal{A}^\ell(q,\omega) = M^{\ell\ell'}(q)\mathcal{A}^{\ell'}(q,\omega). \tag{5.72}$$

The spectrum of excitations is simply found by solving this eigenvalue equation for the matrix $M(q)$.

In order to find the matrix elements $\langle n|\mathcal{A}^\ell(q)|0\rangle$ that enter in susceptibilities we need the following scheme. Assume that the Hamiltonian is of the form

$$H = \sum_{qn} \omega_{qn} \alpha_{qn}^\dagger \alpha_{qn} \tag{5.73}$$

where the sum over q runs over momenta, and n indicates the different excited states. Now $\alpha_{qn}^\dagger$ is a creation operator, and irrespective of whether we are dealing with fermions or bosons we have the following equations of motion

$$i\partial_t \alpha_{qn}^\dagger = -\omega_{qn}\alpha_{qn}^\dagger. \tag{5.74}$$

That is: every eigenvector of $M^{\ell\ell'}(q)$ corresponding to a negative eigenvalue can be identified as a creation operator for one of the elementary excitations. However, the eigenvalue equation itself is not enough because it does not yield the proper normalization of $\alpha^\dagger$. Since we have the eigenvector solution

$$\alpha_{qn}^\dagger = \mathcal{U}^{n\ell}\mathcal{A}^\ell(q) \tag{5.75}$$

we can write out the (anti)commutation relation for $\alpha_{qn}^\dagger$ in terms of the (anti)commutation relations for the $\mathcal{A}^\ell(q)$. Upon requiring that on the mean field level the operators $\alpha_{qn}^\dagger$ obey canonical commutation relations, that is for bosons

$$\left\langle \left[\alpha_{qn}, \alpha_{qn'}^\dagger\right] \right\rangle = \delta_{nn'}, \tag{5.76}$$

we obtain a proper normalization for the new creation operators. We can invert the normalized matrix $\mathcal{U}^{n\ell}$ to express $\mathcal{A}^{\ell}(q)$ in terms of the creation operators $\alpha^{\dagger}_{qn}$. Finally, using $\langle n'|\alpha^{\dagger}_{qn}|0\rangle = \delta_{nn'}$ we can compute the wanted matrix element for $\mathcal{A}^{\ell}(q)$.

As an example of this technique we can compute the matrix element $|\langle n|S^{+}(q)|0\rangle|^2$ for the **antiferromagnetic Heisenberg model** on a square lattice. The mean field ground state is the Néel state, which leads to the following equations of motion,

$$i\partial_t \begin{pmatrix} S^{+}_{qA} \\ S^{+}_{qB} \end{pmatrix} = \frac{1}{2} Jz \begin{pmatrix} 1 & \gamma_q \\ -\gamma_q & -1 \end{pmatrix} \begin{pmatrix} S^{+}_{qA} \\ S^{+}_{qB} \end{pmatrix}. \tag{5.77}$$

where the subscript A and B denote the two different sublattices, and $\gamma_q = \frac{1}{2}(\cos q_x + \cos q_y)$. We quite easily infer that the eigenvalues are

$$\omega_q = \pm \frac{1}{2} Jz \sqrt{1-\gamma_q^2} \tag{5.78}$$

and thus we have one eigenvector corresponding to a creation operator, and one to an annihilation operator. If we define

$$\begin{pmatrix} \alpha^{\dagger} \\ \beta \end{pmatrix} = \mathcal{U} \begin{pmatrix} S^{+}_{qA} \\ S^{+}_{qB} \end{pmatrix} \tag{5.79}$$

then the commutation relations tell us that the eigenvector matrix $\mathcal{U}$ must satisfy

$$1 = \langle [\alpha, \alpha^{\dagger}] \rangle = -2u_{11}^2 \langle S^z_A \rangle - 2u_{12}^2 \langle S^z_B \rangle = -u_{11}^2 + u_{12}^2. \tag{5.80}$$

The initial S^{+}_{q} operator, which enters in the spin susceptibility, can be expressed in terms of the eigenvector matrix as

$$\mathcal{S}^{+}_{q} = \frac{1}{\sqrt{2}} (1\ 1)\ \mathcal{U}^{-1} \begin{pmatrix} \alpha^{\dagger} \\ \beta \end{pmatrix}. \tag{5.81}$$

Some straightforward algebra now yields

$$\left|\langle n|S^{+}(q)|0\rangle\right|^2 = \frac{1}{2} \sqrt{\frac{1-\gamma_q}{1+\gamma_q}} \tag{5.82}$$

which is the same susceptibility one can obtain by using the Holstein-Primakoff linear spin wave approximation. The approximation scheme we introduced here can therefore be viewed as a *generalization of the linear spin wave approximation*.

Let us now apply this technique to the XXZ **model** of section 5.2.1. The Heisenberg equations of motion are

$$\begin{aligned} i\partial_t E_i^+ &= -t\sum_\delta E_i^z E_{i+\delta}^+ + \mu E_i^+ - V_I \sum_\delta E_i^+ E_{i+\delta}^z, \quad (5.83)\\ i\partial_t E_i^- &= t\sum_\delta E_i^z E_{i+\delta}^- - \mu E_i^- + V_I \sum_\delta E_i^+ E_{i+\delta}^z, \quad (5.84)\\ i\partial_t E_i^z &= -\frac{1}{2}t\sum_\delta \left(E_i^+ E_{i+\delta}^- - E_i^- E_{i+\delta}^+\right), \quad (5.85)\end{aligned}$$

where δ runs over all nearest neighbors. These equations cannot be solved exactly, hence we use an approximation based on the mean field results. Products of operators on different sites are replaced by[49]

[49] Zubarev, 1960; and Oles et al., 2000

$$A_i B_j \to \langle A_i\rangle B_j + A_i\langle B_j\rangle \quad (5.86)$$

where $\langle\ldots\rangle$ denotes the mean field expectation value. By such a decoupling the Heisenberg equations of motion become a coupled set of linear equations which can be solved easily. In the homogeneous phase we thus obtain, after Fourier transforming,

$$\begin{aligned} \omega_k E_k^+ &= -\frac{1}{2}tz\left(\cos 2\theta\gamma_k E_k^+ + \sin 2\theta E_k^z\right) + \mu E_k^+ \\ &\quad -\frac{1}{2}V_I z\left(\cos 2\theta E_k^+ + \sin 2\theta\gamma_k E_k^z\right) \quad (5.87)\\ \omega_k E_k^- &= \frac{1}{2}tz\left(\cos 2\theta\gamma_k E_k^- + \sin 2\theta E_k^z\right) - \mu E_k^- \\ &\quad +\frac{1}{2}V_I z\left(\cos 2\theta E_k^- + \sin 2\theta\gamma_k E_k^z\right) \quad (5.88)\\ \omega_k E_k^z &= -\frac{1}{4}tz\sin 2\theta(1-\gamma_k)\left(E_k^+ - E_k^-\right). \quad (5.89)\end{aligned}$$

We can find an analytical expression for the excitations in the superfluid phase,

$$\begin{aligned} \omega_k &= \frac{1}{2}zt\sqrt{1-\gamma_k}\sqrt{1-\gamma_k(1-2\rho)^2 + \frac{4V_I}{t}\gamma_k(1-\rho)\rho}\\ &= \frac{1}{2}zt\sqrt{\rho(1-\rho)(1+V_I/t)}\,|k| + \ldots \quad (5.90)\end{aligned}$$

where $\gamma_k = \frac{1}{2}(\cos k_x + \cos k_y)$. For small momenta this excitation has a linear dispersion, conform to the Goldstone theorem requiring a massless excitation as a result of the spontaneously broken $U(1)$ symmetry. Exactly at $\mu = \mu_c$ the dispersion reduces to $\omega_k = zt\sqrt{1-\gamma_k^2}$, hence the gap at $k = (\pi,\pi)$ closes thus signaling a transition towards the checkerboard phase.

At the critical point and in the checkerboard phase, we need to take into account the fact that expectation values of operators differ on the two sublattices. The Heisenberg equations of motion now reduce to six (instead of three) linear equations. This is technically more difficult but does not pose a real mathematical challenge.

5.2.5 *Collective modes and susceptibilities*

Each phase of the excitons in a strongly correlated bilayer has distinct **collective modes**, by which we can experimentally probe the system. In order to obtain the dispersions of the collective modes we employ the technique of the Heisenberg equations of motion, introduced in the previous section 5.2.4. In the case of the exciton $t - J$ model, however, the set of equations is so large that analytical solutions can in general not be obtained. Whenever necessary, we compute the dispersions numerically.

The dispersions itself are not directly experimentally relevant: one measures **dynamical susceptibilities**. Amongst others, we are interested in the absorptive part of the dynamical magnetic susceptibility, defined by

$$\chi''_S(q,\omega) = \sum_n \langle\psi_0|\widetilde{S}^-(-q)|n\rangle\langle n|\widetilde{S}^+(q)|\psi_0\rangle\delta(E_n - \omega) \qquad (5.91)$$

Here $|\psi_0\rangle$ is the ground state of the system and $|n\rangle$ are the excited states with energy E_n. This spin susceptibility can be measured with, for example, inelastic neutron scattering.[50] Naturally we can thus define an exciton dynamical susceptibility

[50] Coleman, 2013

$$\chi''_E(q,\omega) = \sum_n \langle\psi_0|E^-_{00}(-q)|n\rangle\langle n|E^+_{00}(q)|\psi_0\rangle\delta(E_n - \omega). \qquad (5.92)$$

We use the operator $E_{00}(q)$ because this amounts to the interlayer dipole matrix element, which is detectable using RIXS,[51] EELS[52] or optical absorption (the latter only for $q = 0$).[53]

[51] Ament et al., 2011
[52] Schnatterly, 1979
[53] Basov and Timusk, 2005

The **three dominant phases** we encountered in our mean field analysis will have distinct magnetic and optical responses. Starting with the antiferromagnetic phase shown in figures 5.10 to 5.12, we observe that this limit of vanishing exciton density has been studied in a far greater detail in section 4.2. This allows us to compare the results of the equations-of-motion method with a full resummation of spin-exciton interactions using the SCBA. In the

condensate phase the interplay between excitonic and magnetic degrees of freedom reaches it climax, which was discussed in section 5.1. Here we discuss some remaining details and the checkerboard phase.

Throughout the following discussion, the model parameters are $J = 125$ meV, $\alpha = 0.04$, $V_I = 2$ eV and a varying t and ρ. In order to visualize the susceptibilities we have convoluted χ'' with a Lorentzian of width 0.04 eV. The color scale in the susceptibility plots is on an arbitrary scale.

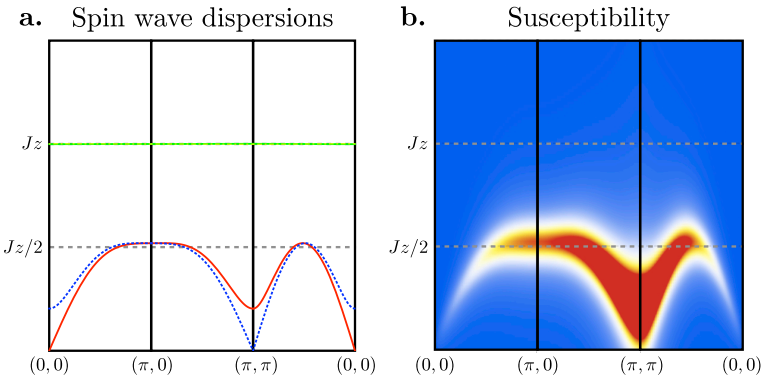

Figure 5.10: The spin wave dispersions (**a.**) and the dynamical magnetic susceptibility (**b.**) in the antiferromagnetic phase. In this phase, the spin wave dispersions are not influenced by exciton dynamics. As is known from previous studies, there are two transversal spin waves and two longitudinal spin waves (Chubukov and Morr, 1995; Rademaker et al., 2012b). The transversal spin waves are gapless around either Γ (solid red line) or the M point (dotted blue line). The longitudinal spin waves, which are associated with interlayer fluctuations (solid green line), are nearly flat and have a gap of order Jz. The dynamic magnetic susceptibility (**b.**) only shows one transversal spin wave. These results and all subsequent figures are obtained using $J = 125$ meV and $\alpha = 0.04$, as is expected for the undoped bilayer cuprate YBCO (Tranquada et al., 1989).

ANTIFERROMAGNETIC PHASE: A SINGLE EXCITON In the limit of zero exciton density we recover the well-known **bilayer Heisenberg** physics. As discussed in section 4.2.1, the spins tend to order antiferromagnetically. The excitations spectrum thus contains a Goldstone spin wave with linear dispersion around Γ and a similar mode centered around (π, π). In addition, the bilayer nature is reflected in the presence of two longitudinal spin waves with a gap of order Jz and a narrow bandwidth of order $J_\perp$. The excitation spectrum and the corresponding magnetic dynamical susceptibility is shown in figure 5.10.

The dynamics of an exciton in an antiferromagnetic background has been studied extensively by means of a linear spin-wave self-consistent Born approximation technique (**LSW-SCBA**) in section 4.2.2. The non-interacting equations of motion method used in this section is certainly less accurate than the full LSW-SCBA computation. However, the mere existence of LSW-SCBA results allows us to compare it with our current non-interacting

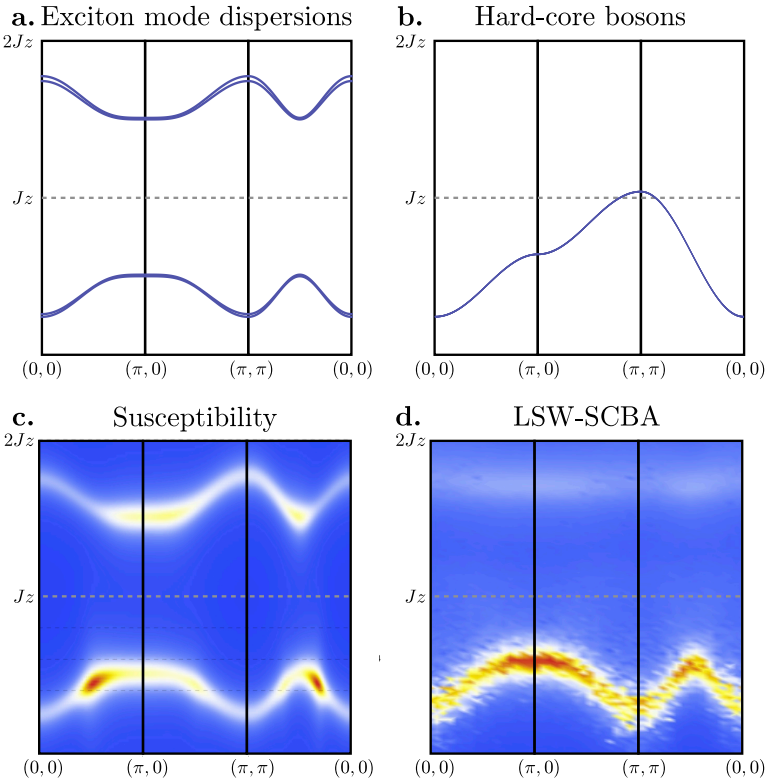

Figure 5.11: The exciton modes in the antiferromagnetic phase in the adiabatic regime $t \ll J$. Here we have chosen $t = 0.1$ eV, $J = 125$ meV and $\alpha = 0.04$. Within the equations of motion picture there are four exciton modes (**a.**), which come in pairs of two with a small interlayer splitting. Due to the antiferromagnetic order the exciton bands are renormalized with respect to a free hard-core boson (**b.**). The susceptibility corresponding to the free exciton motion (**c.**) is verified by the fully interacting LSW-SCBA results (**d.**). This is to be expected: in the adiabatic regime spins react much faster than the exciton motion and the exciton still moves freely dressed by a spin polaron, reducing its bandwidth to order t^2/J.

calculations.

The equations-of-motion method **ignores the interaction** corrections such as dynamical frustration. It treats the excitons as well-defined quasiparticles. As such we can already guess beforehand that the non-interacting results will only be reliable in the adiabatic regime $t \ll J$. Indeed, in the equations-of-motion method we find four exciton modes corresponding to either the singlet E^+_{00} or $m = 0$ triplet exciton E^+_{10} operator, just as in the LSW-SCBA. When $\alpha \to 0$ we can write out an analytical expression for the non-interacting dispersions,

$$\omega_{k,\pm} = \mu \pm \frac{1}{2}\sqrt{(Jz)^2 + \left(\frac{1}{2}zt\gamma_k\right)^2}. \tag{5.93}$$

where each branch is twofold degenerate. This degeneracy is lifted when $\alpha \neq 0$, leading to a splitting of order α which is largest around Γ and M.

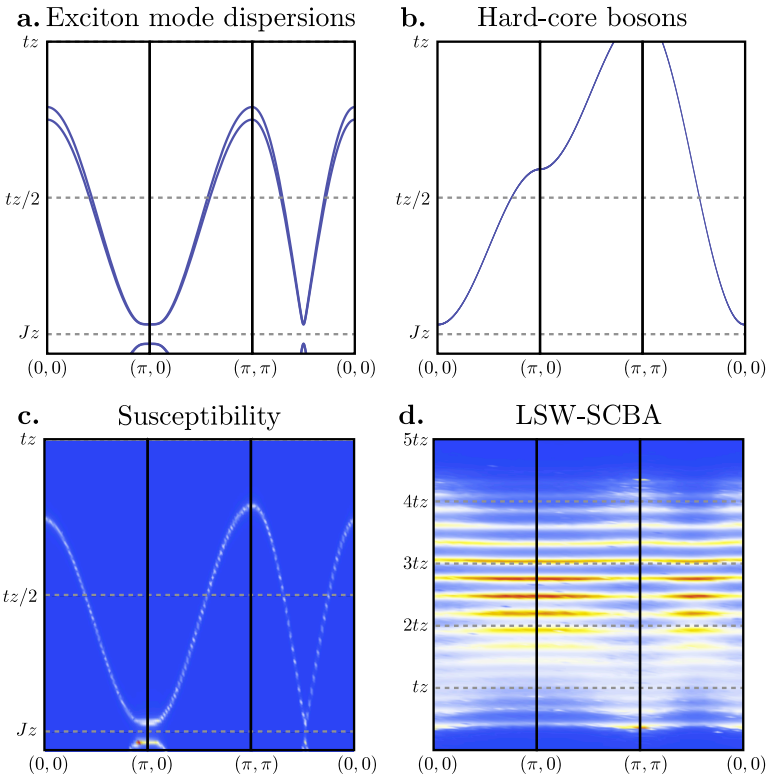

Figure 5.12: The exciton modes in the antiferromagnetic phase in the anti-adiabatic regime $t \gg J$. Here we have chosen $t = 2$ eV, $J = 125$ meV and $\alpha = 0.04$. Just like in figure 5.11 we find four exciton bands (**a.**), renormalized with respect to the free hard-core boson results (**b.**). However, upon inclusion of the interaction the free susceptibility (**c.**) gets extremely renormalized (**d.**). The large exciton kinetic energy together with the relatively spin dynamics create an effective potential for the exciton: the exciton becomes localized and the confinement generates a ladder spectrum. Note that thus in the anti-adiabatic regime the free results (**a.**, **c.**) cannot be trusted.

In the limit of $t \ll J$ the dispersions (5.93) indeed result in an effective exciton bandwidth of order t^2/J, conform the LSW-SCBA as can be seen in figure 5.11. The natural question then arises: how is it possible that in the present non-interacting theory the exciton bandwidth depends on the spin parameter J? For sure, the effective exciton model introduced in section 5.2.1 has no such renormalisation as is shown in figure 5.11. There the exciton bandwidth fully depends on zt.

However, it is important to realize that the exciton operators $E^{+}_{s0,i}$ do not commute with the antiferromagnetic order parameter operator $\widetilde{S}^{z}_{i}$. As a result the mean field energy of exciting an exciton is shifted either up or down (depending on the sublattice) yielding a gap between the two exciton branches of $\mathcal{O}(Jz)$. Now for small t, propagation of the exciton requires that one has to 'pay' the energy shift Jz to move through both sublattices. As a result the effective hopping is reduced by a factor t/J. Therefore the

exciton bandwidth renormalisation, seen in the full LSW-SCBA, is already present at the mean field level.

For large t/J, however, we will pay a price for the convenience of the non-interacting equations of motion method. At mean field level one still expects the dispersions to be (5.93), however, upon inclusion of the interaction corrections this picture breaks down completely. The bandwidth of the non-interacting exciton is of order zt, whereas in the interacting theory an incoherent ladder spectrum of the same width arises. Thus for large t/J the non-interacting results cannot be trusted. However, this only applies to the antiferromagnetic phase due to the presence of dynamical frustration. In general one can say that the non-interacting results are qualitatively correct in the absence of gapless modes that need to be excited in order for an exciton to move. This condition is naturally met for the other two phases, and hence we expect that exciton-spin interactions only lead to qualitative changes in the antiferromagnetic phase.

By simple selection rules one can already conclude that the singlet exciton mode couples to light. As a consequence this is the mode that is visible in the **susceptibility**, as seen in figures 5.11d (for $t < J$) and 5.12d (for $t > J$).

Finally, note that at the transition from the antiferromagnetic phase to the checkerboard phase the gap in the exciton spectrum vanishes at (π, π).

SUPERFLUID PHASE The mode spectrum of superfluid phase, shown in figures 5.13 and 5.14, is characterized by a **linearly dispersing Goldstone mode** associated with the broken $U(1)$ symmetry. This superfluid phase mode has vanishing energy at the Γ point, where we find the inescapable linear dispersion relation

$$\omega_k = \frac{1}{4\sqrt{2}} zt \sqrt{(1-\rho)\rho\,(1+2V_I/t)}\,|k| + \ldots \tag{5.94}$$

The speed of the superfluid phase mode is the same as for the XXZ model in equation (5.90) up to a rescaling of the t and V_I parameters. Indeed, this speed is proportional to the superfluid density $\sqrt{\rho_{\mathrm{SF}}} = \sqrt{\rho(1-\rho)}$. This mode can be seen in the exciton susceptibility, figures 5.13e and f. The Goldstone mode has a gap at (π, π) which decreases monotonically with increasing exciton density. Precisely at the first order transition towards the

checkerboard phase this gap closes.

Next to the Goldstone mode there are two triplet excitations, shown in figure 5.14, each one three-fold degenerate. The degeneracy obviously arises from the standard triplet degeneracy $m = -1, 0, +1$. The two branches, however, distinguish between **exciton-dominated** modes and **spin-dominated** modes, let us discuss them separately.

The spin-dominated modes have a gap of order $\Delta_S = Jz\sqrt{\alpha(1+\alpha-\rho)}$, which is similar to the triplet gap in the bilayer Heisenberg model for large α. However, the bandwidth of these excitations scales with t rather than with J, as would be customary in a system without exciton condensation (see figures 5.14a and b). We discussed these modes in great detail in section 5.1, so let us continue onto the other branch of triplets.

The other branch of triplet excitations is dominated by **triplet excitons**, and is therefore barely visible in the spin susceptibility and not visible in the exciton susceptibility (which only shows singlet excitons). That it is indeed dominated by triplet excitons can be inferred from computing the matrix elements of the operator E_{1m}, as is done in figures 5.14g and h. Furthermore, the gap $\Delta_E = (V_I z + tz)\rho - \mu$ is a function of exciton model parameters only. The bandwidth of this mode is of order $\mathcal{O}(zt)$, relatively independent of the exciton density. As a result, for large superfluid densities the exciton-dominated modes cross the spin-dominated triplet modes. One can directly see this in the excitation spectrum for $\rho = 0.27$ as shown in figure 5.14d.

We can compare the triplet spectrum to the mode spectrum of the singlet phase of the bilayer Heisenberg model. When $J_\perp \gg J$ the ground state consists of only rung singlets. The excitation towards a triplet state, shown in figures 5.14a and b, has a gap $Jz\sqrt{\alpha(\alpha-1)}$ and a bandwidth of order Jz, which is considerably smaller than the $\mathcal{O}(zt)$ bandwidth in the condensate. However, because the topology of the triplet mode is the same we expect that the effect of the spin-exciton interactions is the same in the bilayer Heisenberg model as for the superfluid. Since earlier LSW-SCBA showed no changes in the spectrum due to interactions, we infer that the non-interacting results for the superfluid are reliable.

To conclude our review of the excitations of the superfluid phase we want to discuss the influence of the **interlayer tunneling**. In the context of the XXZ model we noticed that interlayer

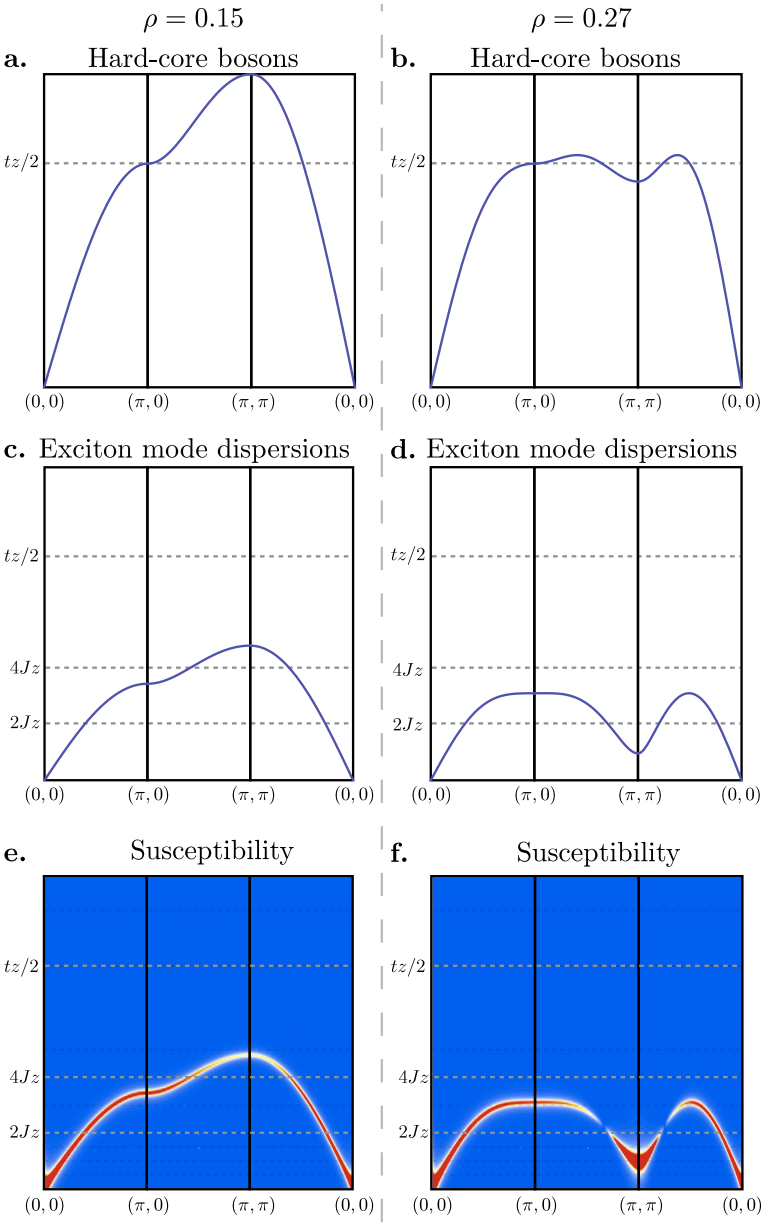

Figure 5.13: Dispersions and susceptibility of the Goldstone mode associated with the exciton condensate. We have set $t = V_I = 2$ eV, $J = 125$ meV and $\alpha = 0.04$, and the exciton density is either $\rho = 0.15$ (left column) or $\rho = 0.27$ (right column). **a, b.** In the simple hard-core boson model the condensate phase clearly show the superfluid phase mode, linear at small momenta. **c,d.** In the full $t-J$ model the Goldstone mode has a similar dispersion as in the XXZ model. The speed of the mode scales with the superfluid density. At higher densities the mode softens around (π, π), and when this gap closes a first order transition to the checkerboard phase sets in. **e,f.** The absorptive part of the exciton susceptibility, which can be measured with for example EELS or RIXS.

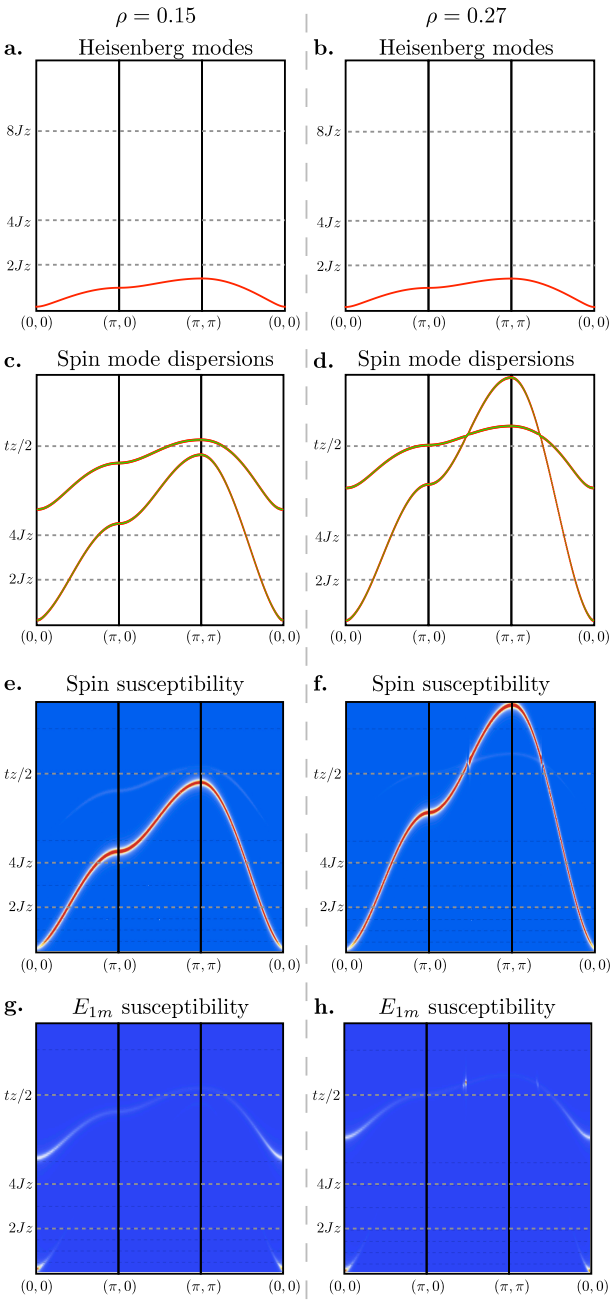

Figure 5.14: Dispersions and magnetic susceptibilities of the exciton condensate. We have set $t = V_I = 2$ eV, $J = 125$ meV and $\alpha = 0.04$, and the exciton density is either $\rho = 0.15$ (left column) or $\rho = 0.27$ (right column). **a,b.** As the exciton condensate is spin singlet, we assume that the excitation spectrum is governed by propagating triplet modes. These modes have a gap of order $J_\perp$ and a bandwidth of order Jz. **c,d.** In contrast to the simple Heisenberg results, the actual triplet modes have enhanced kinetics, see section 5.1. The modes are split in a spin-dominated branch with small gap and large bandwidth proportional to the superfluid density (**e,f.**); and an exciton-dominated branch with a large gap and a small bandwidth (**g,h.**).

tunneling has no qualitative influence on the phase diagram itself. However, the presence of a weak interlayer tunneling may act as phase pinning[54] which opens a gap in the superfluid phase mode spectrum of order $\mathcal{O}(\sqrt{t_\perp(V_I+t)})$. Persistent currents can still exist, but one needs to overcome this gap in order to get the exciton supercurrent flowing.

[54] See section 2.2.2 and Rademaker et al., 2011.

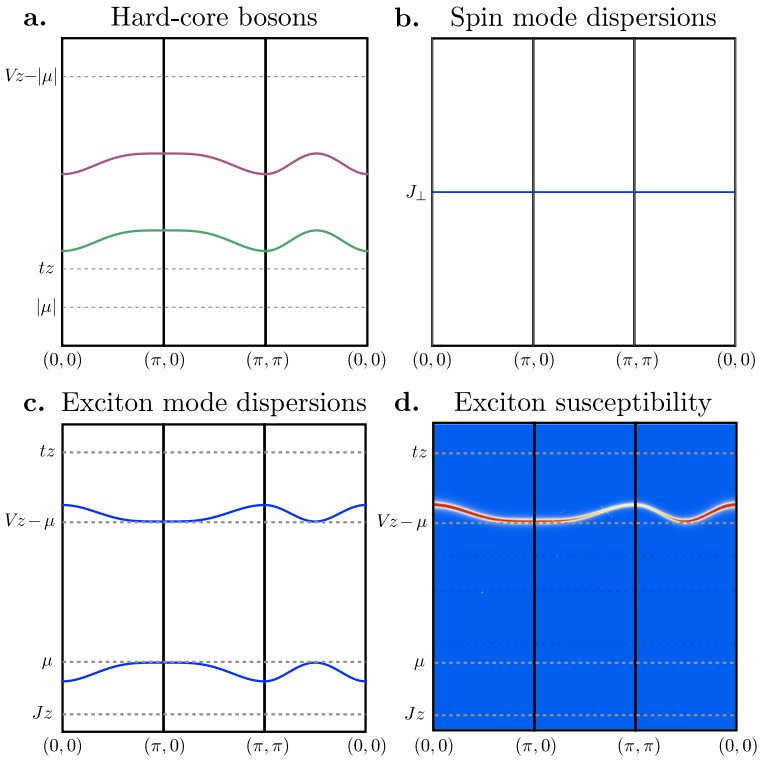

Figure 5.15: The excitation spectrum of the checkerboard phase. **a.** In the simple hard-core boson model there are two exciton modes associated with the 'doublon' and the 'holon' excitation. **b.** The spin modes are decoupled from the exciton modes in the full $t-J$ model. There is only one possible spin excitation: changing the singlet ground-state into a non-propagating triplet. **c.** The exciton modes, on the other hand, can still propagate. The excitation of removing an exciton can propagate through the checkerboard. **d.** The propagating mode that changes an exciton into a singlet is detectable by optical means and thus shows up in the exciton susceptibility.

CHECKERBOARD PHASE The third homogeneous phase of the exciton $t-J$ model is the checkerboard phase. In this phase the unit cell is effectively doubled with one exciton per unit cell. This state is analogous to a **Bose Mott insulator**. The trivial excitations are then the doublon and the holon: create two bosons per unit cell which costs an energy $V_I z-\mu$ or to remove the boson. The latter will generate a propagating exciton mode, with dispersion

$$\omega_{k,pm}=\frac{1}{2}\left(\pm V_I z+\sqrt{(V_I z)^2\pm\left(\frac{1}{2}zt\gamma_k\right)^2}\right)\mp\mu\pm J_\perp. \quad (5.95)$$

There are two such propagating modes: one associated with the **singlet exciton** and one with the triplet exciton. Precisely at the transition towards the superfluid phase, one of these exciton waves becomes gapless. Note that the arguments that lead to the bandwidth renormalisation in the antiferromagnetic phase also apply here, leading to an exciton bandwidth of order t^2/V_I. The dispersions and the corresponding exciton susceptibility can be seen in figure 5.15.

In the spin sector one can excite a **localized spin triplet** on the empty sublattice. The triplet gap is set by the interlayer energy $J_\perp$, and the dispersion is flat because this triplet cannot propagate, as can be seen in figure 5.15b.